J. Fluid Mech. (1996), vol. 318, pp. 339–372

The diffusion of conserved and reactive scalars behind line sources in homogeneous turbulence

By J. D. LI† AND R. W. BILGER

Department of Mechanical and Mechatronic Engineering, The University of Sydney, NSW 2006, Australia

(Received 13 December 1994 and in revised form 6 February 1996)

Experimental results for the statistics of turbulent reactive plumes behind line sources are given. The results are obtained with sufficient spatial and time scale resolution and cover the near and far fields. The results for the conserved scalar, which is constructed from the two reactive scalars, are consistent with those measured in passive thermal plumes. The results for the reactive scalars show that within the experimental range, turbulent mixing is the dominant contributor to the spread rate of the plume and the contribution from chemical reaction is small. However it is found that chemical reaction has a large effect on the decay of the plume reactant concentration and this effect depends on the stoichiometric mixture fraction. The gradient model for turbulent diffusion and the conventional model for the dissipation time scale of scalar variance have been tested and it is found that they are satisfactory in the far field of the plume. However large errors can result in the near field. Also it is found that the turbulent diffusitivities derived from the conserved and reactive scalars are about the same. Various models for the mean chemical reaction rate have been checked and it is concluded that an interpolation between the frozen and equilibrium limits for the covariance of the two reactive scalars will model the mean chemical reaction rate reasonably well.

1. Introduction

Understanding the diffusion of conserved and reactive scalars behind a line source in a homogeneous turbulent flow field has important applications in engineering and meteorology. Many observations of the diffusion behind a line source in homogeneous turbulence have been made using a small temperature difference as a passive conserved scalar‡. These include Uberoi & Corrsin (1953), Townsend (1954), Warhaft (1984) and Stapountzis *et al.* (1986), to mention a few. In many applications the scalars released (such as those from an industrial vent) are reactive. So far the effect of chemical reaction on the diffusion of reactant scalars downstream of a line source has not been studied extensively, and comprehensive experimental data with sufficient resolution are lacking. This is due to the difficulties in measuring the reactive scalars in a turbulent reacting plume with sufficient spatial and temporal resolution and in

† Present address: Department of Mechanical Engineering, Victoria University of Technology, PO Box 14428, MMC, Melbourne, Victoria 3000, Australia.

‡ In this paper, we call a scalar which does not affect the fluid mechanics 'passive' and that which is not affected by chemical reaction 'conserved'. Because the chemical concentrations of the reactive scalars used in this study are low, the heat release from the reaction will have a negligible effect on the temperature rise. Thus all the scalars (reactive and conserved) are passive scalars.

introducing the reactant through the line source without significantly disturbing the flow field.

The available experimental results for a conserved scalar behind a line source reveal the difficulties that one faces in modelling the turbulent plume. These include the failure of the conventional gradient model due to the fact that the length scale of the mean scalar field in the initial stage of the plume development is less than the length scale for turbulence (Corrsin 1974), and the inadequacy of modelling the time scale for scalar dissipation as being proportional to the time scale for turbulent dissipation (Sykes, Lewellen & Parker 1984; Anand & Pope 1985). Deardorff (1978) shows that when the first-order gradient modelling fails, it is likely that the second- and third-order gradient modelling will also fail in predicting the development of the plume in homogeneous turbulence. Similar conclusions can also be expected for reactive scalars.

Because of the difficulties in the conventional modelling of turbulent plumes, a Lagrangian stochastic model based on two-point displacement has been proposed by Durbin (1980) and extended by Sawford & Hunt (1986) and Thomson (1990). The model can predict the mean profile of the conserved scalar and the spread rate of the plume. For the r.m.s. of the conserved scalar, different predictions are obtained with these models. Simpler models for the r.m.s. and higher moments are available from the work of Chatwin & Sullian (1990), Sawford & Sullian (1995) and Mole & Clarke (1995). Komori *et al.* (1991) have attempted to incorporate chemical reaction into the stochastic model but the assumptions made are very limiting and a satisfactory model is yet to be developed. The difficulty of modelling the chemical reaction rate in turbulent reacting flow is well known and many models have been proposed. So far none of the existing models is satisfactory.

In this study nitric oxide (NO) and ozone (O_3) have been chosen as the reactive scalars owing to their easy availability, their simple kinetics and their importance in producing pollution in the atmosphere. The cross-sectional dimension of the line source is one order of magnitude smaller than the length scale of the energy-containing eddies of the grid turbulence. The measurement system can resolve not only the energy-containing and variance-bearing eddy scales but also the energy and variance dissipation eddy scales. The aim of this work is to present experimental data for conserved and reactive scalars in turbulent reactive plumes downstream of line sources and to test some of the various models used in the literature.

The paper is arranged as follows. In §2 the experimental set-up is described and this is followed by presentation of the experimental data in §3, the results for the conserved scalar being given first and compared with results obtained using non-reactive passive scalars. By making such a comparison, validation of our results in the present turbulent reactive plume may be obtained. The statistical results for the reactive scalars are then presented and the effect of the chemical reaction on the spread of the plume and the decay of the plume reactant are discussed. Turbulent flux results are then presented and the gradient model is tested. Finally the problems associated with modelling the scalar dissipation and chemical reaction rate are addressed. In §4 we draw some conclusions.

2. Experimental set-up

The experiments for the diffusion of conserved and reactive scalars behind line sources were carried out in the Turbulent Smog Chamber (TSC) at the University of Sydney, which has been used in previous studies of a turbulent reacting scalar

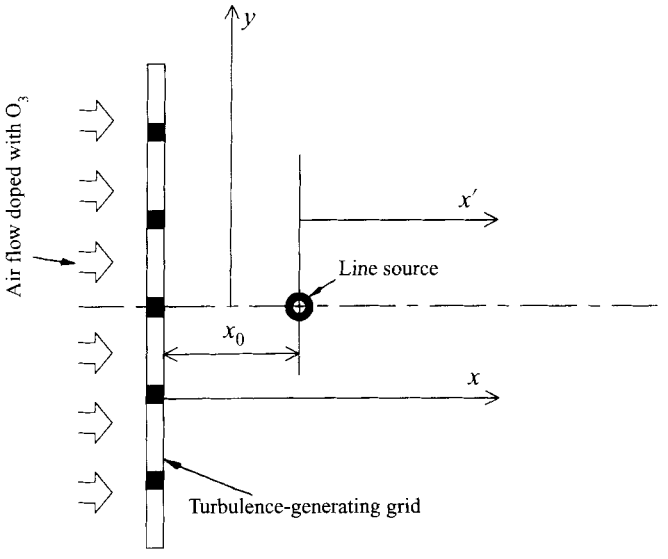

FIGURE 1. Schematic diagram of experimental lay out.

mixing layer (Bilger, Saetran & Krishnamoorthy 1991; Li & Bilger 1993, 1994). The turbulence-generating grid is made of 63 × 63 mm hollow-section aluminium and the mesh length, M, is 320 mm square pitch giving an open area of 65%. The test section of the TSC is 8 m long with a diameter of 2.8 m. The nominal mean velocity used is 0.5 m s^{-1} giving a Reynolds number $Re = UM/\nu \approx 10700$, where U is the mean velocity and ν is the kinematic viscosity.

Nitric oxide (NO) was released from a 2.6 m long stainless steel tube with an outer diameter of 30 mm. Premixed nitrogen and nitric oxide gases were introduced into the tube through one end. Fine mesh inserted into the tube was used to ensure that the outflow is uniform along the tube. The other end of the tube was blocked. The tube was drilled with 250 holes along it. The holes were uniformly distributed with a diameter of 1 mm each. The tube was installed at the centre of the TSC and at $x_0 = 0.425$ m and 2.465 m from the grid, respectively, with the holes facing downstream. Figure 1 shows a sketch of the experimental set-up with the various coordinates defined. The reason for placing the line source at two different distances from the grid is so as to be able to measure the plume in both the 'far field' (for $x_0 = 0.425$ m) and 'near field' (for $x_0 = 2.465$ m).

For reacting plumes, ozone (O_3) was used as the other reactive species in the ambient flow. The ozone was introduced at the inlets of the blowing fans and the concentration was uniform at the cross-sections where the line sources were located. Nitric oxide and ozone have diffusion coefficients of 0.18 and 0.22 $cm^2\ s^{-1}$, respectively, in air at 25°C and 1 atm. In the absence of significant ultra-violet radiation to drive the back reaction, they undergo the irreversible reaction

$$NO + O_3 \rightarrow NO_2 + O_2 + 200\ \text{kJ mol}^{-1} \tag{2.1}$$

with a rate constant k of 0.37 p.p.m.$^{-1}$s^{-1} at 20 °C (Chameides & Stedman 1977). The concentration used for O_3 was less than 3 p.p.m. and the maximum NO concentration was less than 50 p.p.m. From this it can be shown that the maximum temperature

rise due to the chemical reaction was less than 0.2 °C. The reactions are thus passive and the mixing characteristics should be independent of the concentrations used and whether reaction occurs or not.

In the present experiments, two different types of chemiluminescent analyzers (CLA) were used. One is based on analogue mode operation. It was developed by Mudford & Bilger (1983) and modified by Li, Brown & Bilger (1992). We will call this CLA I. The frequency response of this system is 20 Hz, the signal-to-noise ratio is about 25 and its dynamic range is small. For the present experiment, this system was used to measure the chemical concentrations in the far field. The other CLA system used is based on photon-counting techniques. We will call this CLA II. In comparison with CLA I, it has a higher frequency response (50 Hz), larger dynamic range and smaller signal-to-noise ratio when the signal is weak due to Poisson noise. In the far-field measurement, the NO concentration is low and this system is not suitable. However in the near field where the NO concentration can be very high both instantaneously and on average, CLA I is not suitable owing to its limited dynamic range. CLA II has been used in the near-field measurements. Thus both types of CLA are complementary to each other in the present experiment.

NO calibration was done using a gas cylinder of known concentration, diluted with precision flow meters. The O_3 calibration was determined indirectly by the titration method of Post & Kewley (1978). During calibration, care was taken to make sure that the calibrated ranges of both NO and O_3 concentrations were larger than the maximum concentrations encountered during the measurements. An X-wire probe with a constant-temperature hot-wire-anemometer (HWA) was used to measure the two velocity components. The wires were calibrated statically against a TSI 1125 calibrator. A third-order curve fitting procedure was used to fit the calibration data. The present experimental set-up is a compromise between the need for having a known turbulence field at reasonably high Reynolds number and the need for the CLA to be able to resolve the eddy scales responsible for variance and dissipation. As reported in Li *et al.* (1992) a flow anomaly present in the results of Bilger *et al.* (1991) has been eliminated.

Simultaneous point measurements of two components of velocity and of the two reactant concentrations were taken across the flow field at different downstream stations from the line source. The sampling tube, which has a sonic nozzle at its inlet, was located 18 mm above the hot-wire probe. This is smaller than the Taylor microscale $\lambda(\approx 25$ mm) in the present experiment. It was found that with this separation, the sampling tube did not interfere with the flow field at the hot-wire sensor location. The CLA I samples gas at 140 std. $cm^3\ s^{-1}$ through a Teflon tube of 2.8 mm internal diameter and 3.1 m length. The flow rate for the reactant in excess was 87 std. $cm^3\ s^{-1}$. The pressure inside the reaction cell in front of the photomultiplier tube was 3.5 kPa. The delay time caused by the travelling of the sampled gas through the sampling tube is approximately 63 ms and the spatial resolution of the CLA I is 9.8 mm. The time delay has been corrected for during data processing. Some reaction occurred during the process of delivering the gas from the nozzle to the reaction cell and this was corrected for as suggested by Bilger *et al.* (1991) (The correction is in general less than 1%.) The signals were filtered using a pair of 50 Hz analogue filters and sampled at 128 Hz using a 12 bit A/D converter. From the mass balance, signal-to-noise ratios, spectral densities, record lengths and other information presented in detail elsewhere in the paper, it is expected that the accuracy of mean values is about $\pm 5\%$, that of variance and second-order quantities is about $\pm 10\%$ and that of higher moments (such as kurtosis) $\pm 20\%$.

For CLA II, the gas sampling rate, the flow rate for reactant in excess, and the pressure inside the reaction cell in front the photomultiplier are about the same as for CLA I. The length of the sampling tube was reduced to 30 cm, the spatial resolution of the CLA II is 4.5 mm, the delay time in the sampling tube is small (less than 7 ms) and the reaction occurring in the sampling tube can be neglected. Because CLA II works under photon-counting conditions, the chemical concentration of the sampled gas is proportional to the number of the photons hitting the window in front of the photomultiplier per unit time. The number of photons was counted by an electronic counter and sampled at 128 Hz. Because photon arrival is not continuous, analogue filtering cannot be used to cut off the noise from the signal. Instead a low-pass Butterworth digital filter was applied after the data were sampled. Owing to the Poisson distribution of photon arrival, the signal-to-noise ratio is proportional to $N^{1/2}$ where N is the average number of photons in each sampling time interval Δt. Because the mean chemical concentrations are different at different positions across the flow, the signal-to-noise ratio of the sampled data will also be different (the chemical concentration is proportional to N). In order to choose the order and the cut-off frequency of the filter, a turbulence velocity signal from the hot wire was contaminated with Poisson noise to yield different signal-to-noise ratios. In comparison with the energy spectrum of the original velocity signal, that with added noise becomes constant at high frequency. In order to recover the energy spectral density of the original turbulence signal using the low-pass digital filter, it was found that the cut-off frequency can be chosen as the frequency where the spectral density is twice the constant value found at high frequencies. Unless the signal-to-noise ratio is very low, it was found that a third-order low-pass filter works well. Based on these findings, the sampled raw data of the chemical concentrations were processed first without applying the digital filter. The spectral densities of both the NO and O_3 concentrations were then used to determine the cut-off frequencies corresponding to each chemical species. The data were reprocessed again with the digital filters applied. Figure 2(*a*) shows the spectral densities of both the NO and O_3 concentrations with and without the digital filters at $x'/x_0 = 0.4$ ($x_0 = 2.465$ m) and at the centre of the plume. The signal-to-noise ratios for NO and O_3 concentrations are 12.4 and 13.0 respectively. At high frequencies the spectral densities with digital filters are dominated by the filter characteristics. The effect of applying the digital filter on the mean and r.m.s. values of the chemical concentrations is negligible. However its effect on the variance dissipation is very large as shown in figure 2(*b*), where only the data for the NO concentration have been shown and the results have not been normalized. In presenting figure 2(*b*), Taylor's hypothesis was used and the local isotropy assumption has been made.

The total number of points sampled was 32768 for each measurement, giving a sampling time of 256 s. Given that the frequencies for the energy-containing eddies are about 2 Hz, this represents about 500 eddy turnover times. A test has been performed at $x'/x_0 = 0.4$ ($x_0 = 2.456$ m) and at the centre of the plume. It is found that, with half the sampled number of points (16384), the kurtosis is about 7% different from that obtained with 32768 sampled points and the p.d.f. is indistinguishable from that with 32768 sampled points. At similar flow conditions, Brown & Bilger (1996) have shown that, with a 10 Hz third-order low-pass digital filter, the variance, skewness and kurtosis of both reactants were found to drop by no more than 3% on the centreline. All the data processing was performed on a high-speed PC486.

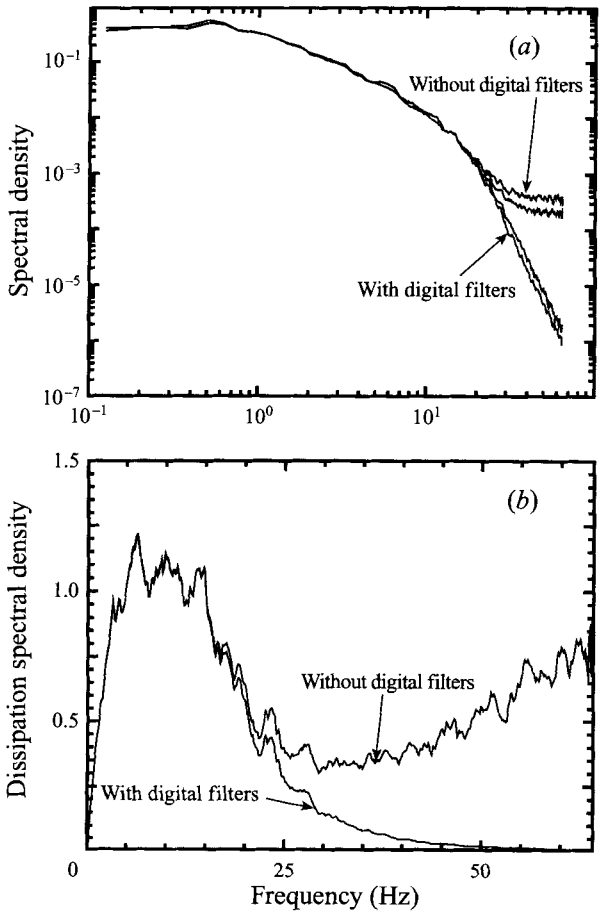

FIGURE 2. Spectral densities of NO and O_3 concentrations with and without applying filters at $x'/x_0 = 0.4$ ($x_0 = 2.465$ m). (*a*) The spectral density; (*b*) the dissipation spectral density for NO concentration.

Following Bilger *et al.* (1991), from the measured concentrations of NO and O_3, a conserved scalar called the mixture fraction can be defined as

$$\xi = \frac{\Gamma_{NO} - \Gamma_{O_3} + \Gamma_{O_{3_2}}}{\Gamma_{NO_1} + \Gamma_{O_{3_2}}} \tag{2.2}$$

where Γ_{NO} is the concentration of NO, Γ_{O_3} the concentration of O_3, $\Gamma_{O_{3_2}}$ is the concentration of O_3 at $y \to \pm\infty$ and Γ_{NO_1} is the concentration of NO at the line source. When $\Gamma_{NO} = \Gamma_{O_3}$, $\xi = \xi_s = \Gamma_{O_{3_2}}/(\Gamma_{NO_1} + \Gamma_{O_{3_2}})$ and this is called the stoichiometric mixture fraction. In the non-reactive scalar experiment, NO was released from the line source with no ozone in the background. In this case the concentration of NO is a conserved scalar, and $\xi = \Gamma_{NO}/\Gamma_{NO_1}$. The Damköhler number, N_D, is defined as

$$N_D \equiv \frac{kM(\Gamma_{NO_1} + \Gamma_{O_{3_2}})}{U}. \tag{2.3}$$

3. Experimental results

3.1. *Velocity field*

The flow field after the grid is near-field grid turbulence. The mean velocity and the r.m.s. of the velocity fluctuations across the flow were checked. The results are similar to those of Jayesh & Warhaft (1992), i.e. beyond $x/M = 4$, the mean and r.m.s. of the velocity profiles were fairly uniform except near the wall of the chamber where a boundary layer was developing. The nominal mean velocity is 0.5 m s^{-1} with a 3% traverse variation. Within $x/M < 4$, inhomogeneity occurs. For the far-field measurement, the line source is located at $x_0/M = 1.33$. Because of this, caution should be taken in interpreting the results. However, the fact that the present experimental data in the far field agree with those from the thermal line source plume (at $x_0/M > 10$) gives support to the validity of the present far-field experimental data. The experimental data show that for $x/M \leqslant 10$, the energy decay exponent is -1.7 and for $x/M \geqslant 10$ it is -1.3. These results are again consistent with those of Jayesh & Warhaft (1992). The length scales of the energy-containing eddies, $l = q^{3/2}/\epsilon$, are 201 mm and 226 mm and the Kolmogorov length scales, $\eta = (\nu^3/\epsilon)^{1/4}$, are 2.42 mm and 2.87 mm at $x/M = 15$ and 21, respectively. Here $q = \frac{1}{2}(\overline{u'^2}+\overline{v'^2}+\overline{w'^2})$ is the kinetic energy of turbulence, u', v' and w' are the three velocity fluctuation components and ϵ is the dissipation rate of the turbulence kinetic energy calculated using $\epsilon = -\mathrm{d}q/\mathrm{d}t$. The flow field was quite anisotropic with $u'/v' \approx u'/w' = 2.1$ and 1.8 at $x_0 = 0.425$ m and $x_0 = 2.456$ m, respectively. The Reynolds number based on the tube diameter of the line source is about 1000 and the vortex shedding frequency from the line source is about 3.3 Hz (Roshko 1954). However it is found that when $x'/M > 1$, there is no difference between the energy spectral densities (at the centre of the wake) with and without the line source (see later).

3.2. *Concentration check*

In order to be confident about the homogeneity of the scalar field in the z-direction and that the plume develops properly downstream, the NO concentration behind the non-reactive plume was checked. It was found that both the mean and the r.m.s. of the NO concentration are uniform along the z-direction within $\pm 5\%$ variation. Because of this we can assume that the scalar field is homogeneous in the z-direction (the velocity field is homogeneous in both the y- and z-directions). For NO released from the line source (non-reactive) the following relationship holds:

$$Q = \overline{U}L \int \Gamma_{NO} \mathrm{d}y = \text{const.} \tag{3.1}$$

The present experimental data show that relationship (4) holds fairly well with a $\pm 5\%$ variation for $0 < x'/M < 20$. In comparison with the similar check of Stapountzis *et al.* (1986) (their figure 11) for a thermal line source, the present effective source strength is essentially constant.

3.3. *Conserved scalar*

Table 1 lists the Γ_{NO_1}, $\Gamma_{O_{3_2}}$, ξ_s, N_D, x'/x_0 and σ_1 (the standard deviation of the plume) for the present experiments. Experiments using NO alone as a non-reactive scalar and using NO and O_3 as reactive scalars have been conducted. The NO and O_3 concentrations were varied such that in general low NO concentration was used when the sampling probe was close to the line source in order to reduce the demand on the dynamic range of the CLA, and high NO concentration was used when the sampling

Symbol	Γ_{NO_1}(p.p.m.)	$\Gamma_{O_{3_2}}$(p.p.m.)	ξ_s	N_D	x'/x_0	σ_1 (mm)	Comments
■	11.9	0			0.75	60.0	Non-reactive
□	11.9	0			1.51	93.0	Non-reactive
▲	32.5	0			3.01	115.0	Non-reactive
△	32.5	0			4.52	145.0	Non-reactive
▼	32.5	0			6.02	180.0	Non-reactive
▽	32.5	0			7.53	200.0	Non-reactive
◆	32.5	0			9.04	215.0	Non-reactive
◇	40.6	0			10.54	235.0	Non-reactive
●	40.6	0			12.05	248.0	Non-reactive
○	40.6	0			13.55	260.0	Non-reactive
A	18.3	1.85	0.092	4.8	1.51	85.0	Reactive
B	18.3	1.85	0.092	4.8	3.01	120.0	Reactive
C	26.9	1.85	0.064	6.8	4.52	150.0	Reactive
D	21.7	1.85	0.079	5.6	6.02	180.0	Reactive
E	21.7	1.22	0.053	5.4	7.53	200.0	Reactive
F	21.7	1.02	0.045	5.4	9.04	205.0	Reactive
G	21.7	1.78	0.076	5.6	10.54	235.0	Reactive
H	15.6	0			0.05	30.2	Non-reactive
I	15.6	0			0.10	43.0	Non-reactive
J	15.6	0			0.20	67.5	Non-reactive
K	12.9	0			0.40	90.0	Non-reactive
L	12.9	0			0.82	130.0	Non-reactive
M	19.5	2.5	0.114	5.2	0.05	31.0	Reactive
N	19.5	2.5	0.114	5.2	0.10	41.5	Reactive
O	19.5	2.4	0.110	5.2	0.20	63.0	Reactive
P	14.8	2.4	0.140	4.1	0.40	85.0	Reactive
Q	14.8	2.3	0.135	4.1	0.82	125.0	Reactive

TABLE 1. Experimental conditions

probe was far away from the line source in order to improve the resolution of the CLA.

The profiles of the mean conserved scalar measured from both the non-reactive and reactive plumes, with the conserved scalar being normalized by its centreline value $\overline{\xi}_c$ and the distance y by the standard deviation σ_1, closely follow a Gaussian form. Figure 3 shows the standard deviation obtained from the mean profiles. In the figure, distance x' from the line source has been normalized by x_0 and $\sigma_y \equiv (\sigma_1^2 - \sigma_0^2)^{1/2}$ by $l_0 (= v'^3/\epsilon)$, which is the length scale of the energy-containing eddies at x_0; $l_0 = 72$ mm and 125 mm at $x_0 = 0.425$ m and 2.465 m, respectively. For $x_0 = 0.425$ m ($x_0/M \approx 1.3$) the line source is located in the transition region of the grid turbulence. The energy decay in this region does not follow a power law (Jayesh & Warhaft 1992, Li *et al.*, 1992) and l_0 is calculated by extrapolating the energy decay law $v^2/U^2 = A(x/M)^{-1.7}$ to $x = x_0 = 0.425$ m. In figure 3, the present experimental data have been corrected for the finite line source size, σ_0. Owing to molecular diffusitivity, $\sigma_0 = 28.5$ mm is larger than the radius of the line source tube. σ_y in the present near-field measurement is slightly higher than that of Warhaft (1984) and Stapountzis *et al.* (1986). The reason for this could be that the present line source size is fairly large ($\approx 12\eta$) and the flow field is not as isotropic as that of Warhaft (1984) and Stapountzis *et al.* (1986) in the thermal plume.

Warhaft (1984) and Anand & Pope (1985) point out that, when the source size is smaller than the Kolmogorov length scale, the evolution of the plume width shows

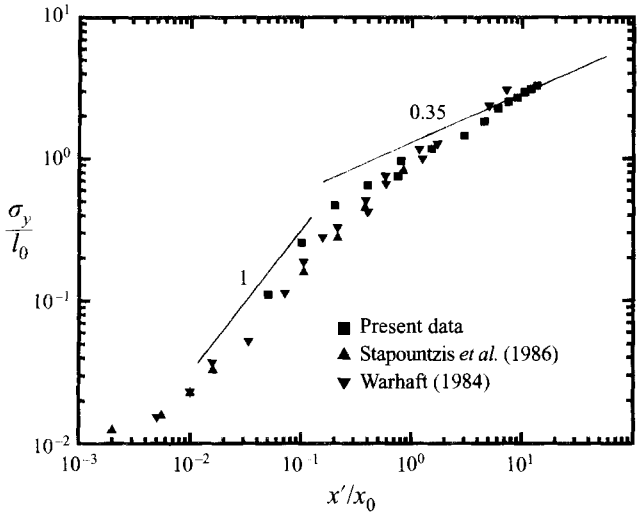

FIGURE 3. The development of the standard derivation of the mean conserved scalar profiles.

three distinct stages: the molecular diffusive stage ($t \ll D/\overline{v^2}$) wherein the plume width increases as $t^{1/2}$, where D is the molecular diffusitivity of the conserved scalar; the turbulent convective stage ($D/\overline{v^2} \ll t \ll t_L$, where t_L is the Lagrangian time scale of the turbulence, see Monin & Yaglom 1975) where the width increases linearly with t; and the turbulent diffusive stage ($t \gg t_L$) where the plume width increases as $t^{1-n/2}$, where n is the decay exponent of $\overline{v^2}$. In figure 3 our data have been compared with those of Stapountzis *et al.* (1986) and Warhaft (1984). The prediction of Anand & Pope (1985) has not been shown here since it agrees with the data of Warhaft (1984).

In the present experiment, the molecular diffusive region corresponds to $x' < 4$ mm. This is much less than the diameter of the line source. Because of this we could not take measurements in the molecular diffusion region. The plume spread rate of a non-reactive scalar, which does not affect the flow field, and that of a conserved scalar, which is not affected by chemical reaction, should be the same since the governing equations and the boundary conditions for the two scalars are the same. It can be seen from figure 3 that in general our results agree with the previous experimental data. Figure 3 also shows that the present experimental data are in the turbulent convective region for the near-field measurements and in the turbulent diffusive stage for the far-field measurements. In the far field the plume width grows as $(x'/x_0)^{0.35}$, as shown in figure 3, and this is consistent with the decay index of -1.3 for the turbulence kinetic energy.

Figure 4(*a*) shows the r.m.s. profiles of the conserved scalar normalized by the centreline values in the near-field measurements and figure 4(*b*) shows the same quantities for the far field. In general the data do not collapse as well as those for the mean conserved scalar. Also it can be seen that the profiles show off-centre peaks in the far field and a central peak in the near field. The experimental data of Warhaft (1984) and the theoretical prediction of Thomson (1990) both show that at large x'/x_0, the r.m.s. profile has off-centre peaks. A close look at the data shows that for $x'/x_0 \leqslant 0.8$ the peak of the r.m.s. profile is at the centre of the plume and when $x'/x_0 \geqslant 1.50$ the profile shows off-centre peaks. This shows that the off-centre peak appears within $0.8 < x'/x_0 < 1.5$. The data of Warhaft (1984) show that the off-centre peak appears at $x'/x_0 \approx 1.93$ and the theoretical result of Thomson (1990)

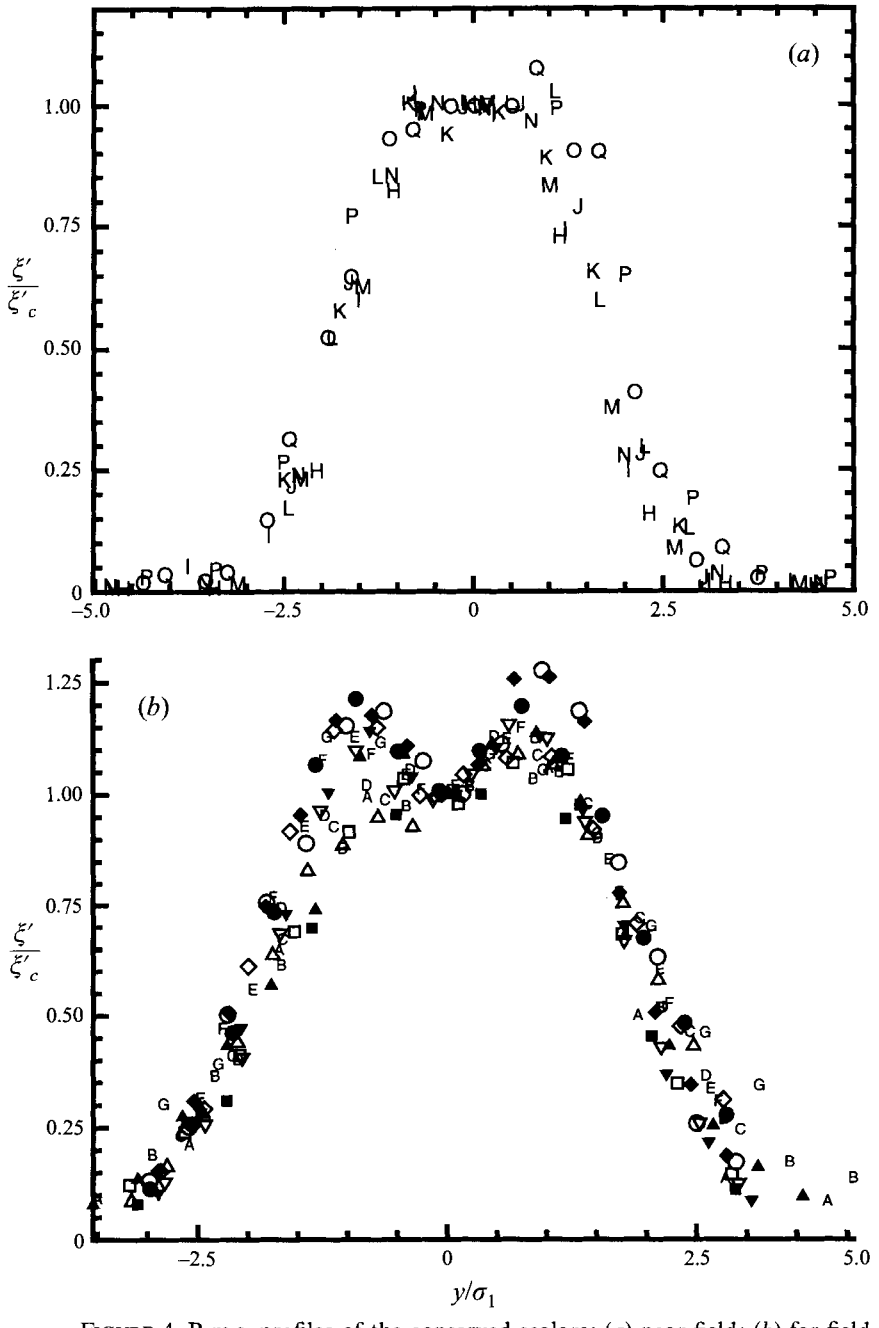

FIGURE 4. R.m.s. profiles of the conserved scalars: (*a*) near field; (*b*) far field. Symbols are listed in table 1.

suggests that the off-centre peaks occur when $x'/x_0 \geqslant 0.43$. The present experimental data are consistent with these earlier results.

Figure 5 shows the r.m.s. values of the conserved scalar (normalized by the centreline mean values) at the centre of the plume. Also shown in the figure are the results of Warhaft (1984) and the theoretical results of Thomson (1990). It seems that the

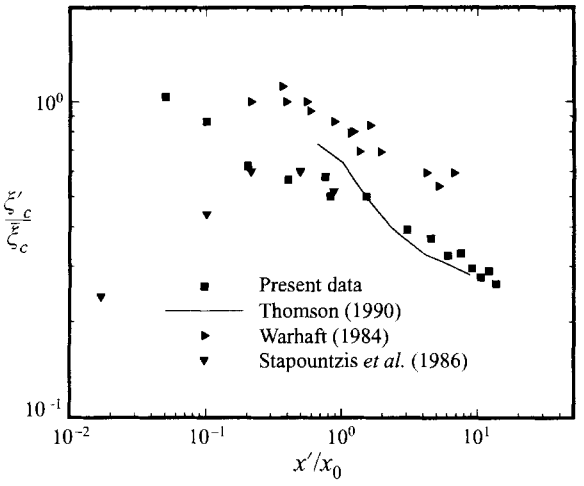

FIGURE 5. The r.m.s. values of the conserved scalar at the centre of the plume.

present near-field results decrease faster than those of Warhaft (1984) and Thomson (1990) (not shown here). For $0.2 < x'/x_0 < 1$, the present results agree with those of Stapountzis *et al.* (1986). In the far field the present results for the normalized r.m.s. values at the centre of the plume are smaller than those of Warhaft (1984) and agree with the theoretical results of Thomson (1990). However, it should be pointed out that the prediction of Thomson (1990) is based on a single turbulent energy decay law ($n = 1.35$); the present far-field plume experiences a turbulent energy decay law of $n = 1.7$ for $x/M < 10$ and of $n = 1.3$ for $x/M > 10$. The data of Warhaft (1984) suggest that the asymptotic value for $\xi'_c/\overline{\xi}_c$ is 0.7, Stapountzis *et al.* (1986) gives 0.5 and Thomson (1990) suggests that it should be 0.16. The present results show that $\xi'_c/\overline{\xi}_c$ is still decreasing at $x'/x_0 > 10$ and the asymptotic value should be less than 0.3.

Stapountzis *et al.* (1986) suggested that vortex shedding (see later) has some effect on the mean and r.m.s. values of the conserved scalar. However this effect is limited to $x'/M < 1$. Their figure 18 shows that although the effect of vortex shedding on the mean decreases very quickly, the finite size of the line source has a long-lasting effect on the centreline r.m.s. value of the conserved scalar. Thus the low r.m.s. values at the centre of the plume in the present experiment, especially those at small x'/x_0, could be due to the large line-source size used.

As pointed out by Warhaft (1984), Stapountzis *et al.* (1986) and Sawford (1992), the profile for the second-order absolute moment has a simpler structure than that for the second-order central moment. The present second-order absolute moments, after being normalized by the centreline value $(\overline{\xi^2})_c$ follow the Gaussian profile with standard deviation σ_2. Figure 6 shows the ratios $(\overline{\xi^2})_c/\overline{\xi}_c^2$ and σ_2/σ_1. In general, $(\overline{\xi^2})_c/\overline{\xi}_c^2$ and σ_2/σ_1 decrease with increasing x'/x_0. It seems that both ratios approach constants at large x'/x_0. From the Lagrangian theory of two-particle dispersion, Stapountzis *et al.* (1986) and Sawford (1992) predict that

$$\overline{\xi}(y) = \frac{Q'}{[2\pi(\sigma_0^2 + \sigma_y^2)]^{1/2}} \exp\left(-\frac{y^2}{2(\sigma_0^2 + \sigma_y^2)}\right) \tag{3.2}$$

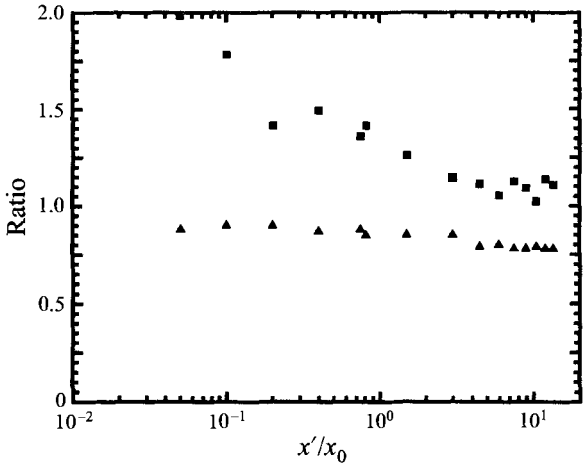

FIGURE 6. The ratios $(\overline{\xi^2})_c/\overline{\xi}_c^2$ (■) and σ_2/σ_1 (▲).

and

$$\overline{\xi^2}(y) = \frac{Q'^2}{[2\pi(\sigma_0^2+\sigma_\Sigma^2)]^{1/2}} \exp\{-\frac{y^2}{(\sigma_0^2+\sigma_\Sigma^2)}\} \int_{-\infty}^{\infty} P(\Delta',0;0,t)S(\Delta')\mathrm{d}\Delta' \qquad (3.3)$$

where Q' is the source strength, Σ is the 'centre-of-mass', Δ is the separation of the particle pairs, $P(\Delta',0;0,t)$ is the transition p.d.f. of the particle pairs which has a separation of Δ' at $t = 0$ and a separation of 0 at t, and S is the distribution of the source. Thomson (1990) shows that σ_y and σ_Σ increase with t and approach the same functional form as $t/t_L \gg 1$. From these it can be easily shown that when $x'/x_0 \to \infty$, both σ_2/σ_1 and $(\overline{\xi^2})_c/\overline{\xi}_c^2$ approach constants. The data in figure 6 support their predictions.

Theoretically the asymptotic value of $\xi_c'/\overline{\xi}_c$ has been shown to depend on the precise form of $P(\Delta)$ in (3.3). Durbin (1980) predicts that $\xi_c'/\overline{\xi}_c$ depends on the source size with $P(\Delta)$ based on inertial range scaling. Sawford & Hunt (1986) include the finite Reynolds number effect and conclude that when the source size is comparable to the Kolmogorov scale, $\xi_c'/\overline{\xi}_c$ becomes independent of source size. Thomson (1990) uses a different form of $P(\Delta)$ and finds that the asymptotic value $\xi_c'/\overline{\xi}_c$ is independent of the source size. The present experiment (or any of the plume experiments in the literature) does not have a test section long enough to settle this theoretical dispute and the results cannot be used to claim support for any particular theory.

Figure 7 shows the skewness and kurtosis of the conserved scalar at various downstream stations. The results show that the skewness is in general larger than zero and that the kurtosis is larger than 3 (which are the values for a Gaussian probability density function, p.d.f.). This means that the p.d.f. of the mixture fraction is skewed towards larger mixture fraction values. For the near-field measurements, the skewness and kurtosis are in general higher than those in the far field for all positions across the plume. In the far-field measurements near the centre of the plume, the skewness approaches zero and the kurtosis approaches a constant of 3. This indicates that the p.d.f. becomes symmetrical and approximately Gaussian. Also the skewness and kurtosis in general collapse together for $|y/\sigma_1| < 2.5$ in the far field. Figure 8 shows the p.d.f.s of the mixture fraction at $x'/x_0 = 0.725$ and 12.0 ($x_0 = 0.425$ m) at the centre of the plume ($y/\sigma_1 = -0.1$) and at some distance from

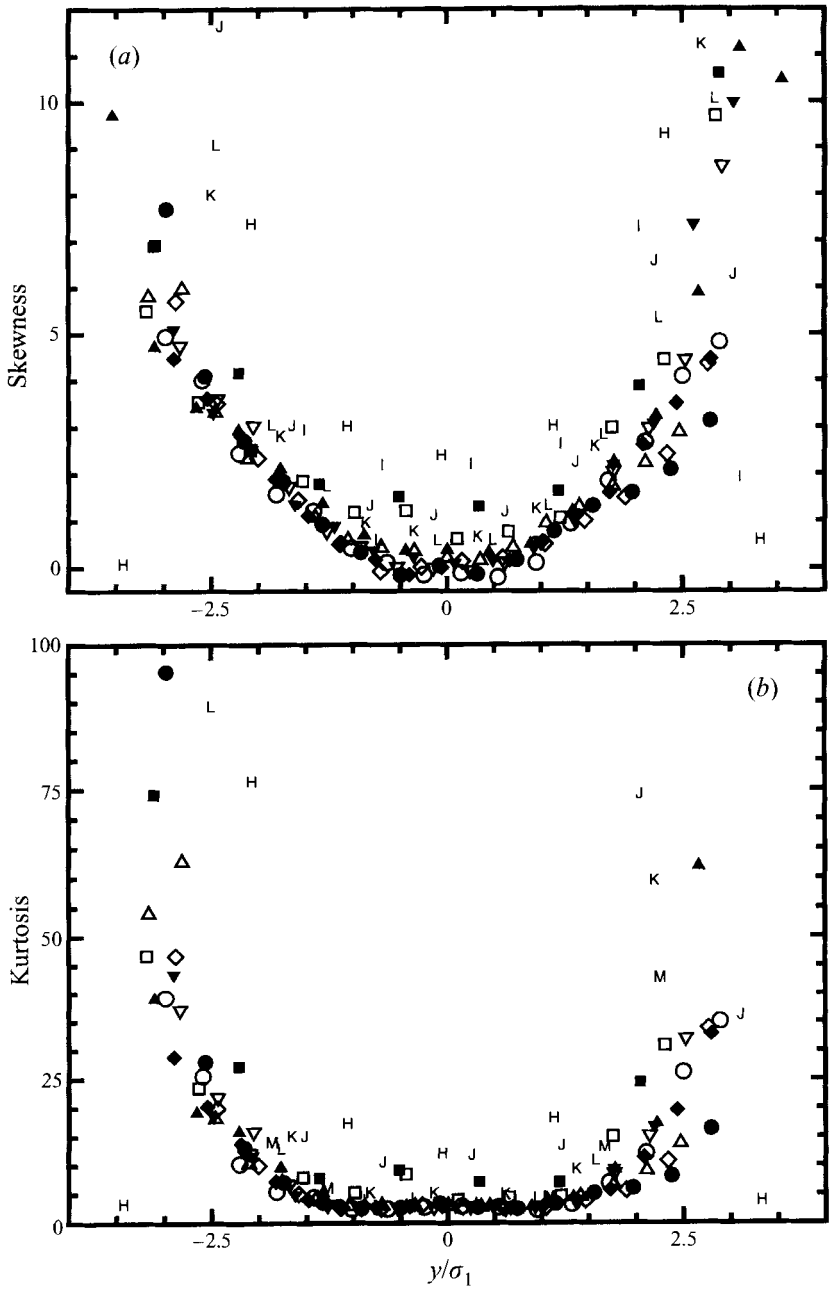

FIGURE 7. (*a*) Skewness and (*b*) kurtosis of the conserved scalars.

the centre of the plume ($y/\sigma_1 \approx -2.5$). In the figure the horizontal axis is $(\xi - \overline{\xi})/\xi'$. At the centre of the plume, the p.d.f. at $x'/x_0 = 0.725$ (figure 8*b*) is skewed towards large mixture fraction values, but that at $x'/x_0 = 12.0$ (figure 8*d*) becomes Gaussian (also shown in the figure). Off the centre, the p.d.f.s at both streamwise positions are very spiky with long tails of positive fluctuations. This is consistent with the results of Fackrell & Robins (1982). In their neutral boundary layer experiment, they find that the p.d.f. is close to Gaussian near the ground far downstream and it

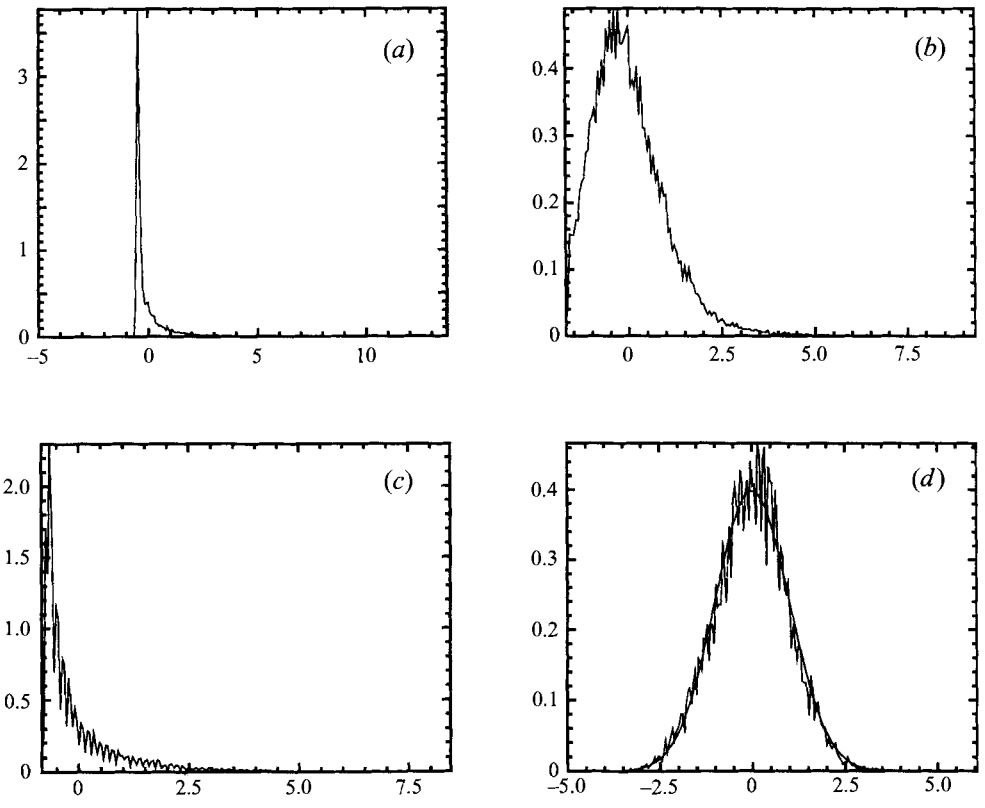

FIGURE 8. The p.d.f.s of the conserved scalar. (*a*) $x'/x_0 = 0.725$, $y/\sigma_1 = -2.5$; (*b*) $x'/x_0 = 0.725$, $y/\sigma_1 = -0.1$; (*c*) $x'/x_0 = 12.0$, $y/\sigma_1 = -2.2$; and (*d*) $x'/x_0 = 12.0$, $y/\sigma_1 = -0.1$. $x_0 = 0.425$ m.

remains 'exponential-like' at the edge of the plume (which is some distance from the ground).

Chatwin & Sullivan (1990) propose a theory which shows that for a wide range of self-similar scalar fields the moments of the probability density of concentration have a very simple form. This theory has been developed further by Sawford & Sullivan (1995) an Mole & Clarke (1995). Mole & Clarke (1995) found that the (K,S) plot collapses and the collapse is onto a quadratic of the form $K = aS^2 + b$. Using the data of Mole & Jones (1994), which were taken in field experiments, they found that $a = 1.31, b = 0.77$. Figure 9 shows the (K,S) plot† from the present expermental results and the data in general collapse together. A best curve fit to the data gives $a = 1.51$ and $b = 2.8$.

Figure 10 shows the measured spectral densities of the v-velocity component and the conserved scalar at $x'/M = 1$ and $12(x_0 = 0.425$ m). The densities have been normalized such that the area under the curve is unity. In figure 10 the v-spectral densities have been shifted by two decades for clarity. The spectrum of the u-velocity component is similar to that of the v—velocity component. The vortex shedding frequency from the 30 mm diameter tube of the line source is about 3.3 Hz (Roshko 1954). Figure 10 shows no energy peak at this frequency even at $x'/M = 1$. However for measurement at $x'/M < 1(x_0 = 2.465$ m), the spectral densities of the

† We are indebted to one of the referees for suggesting this plot.

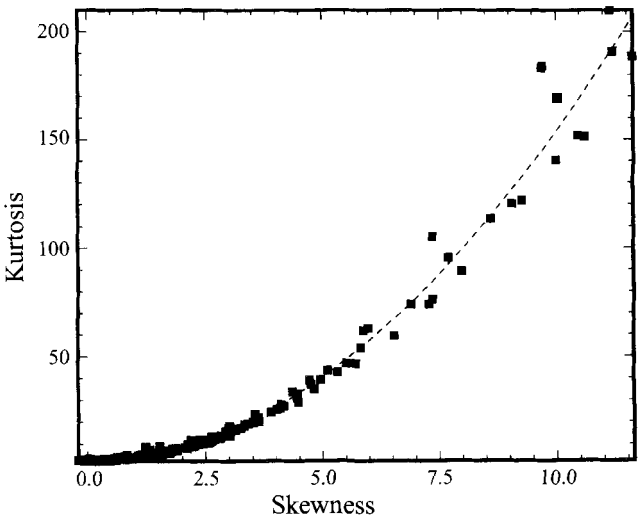

FIGURE 9. The kurtosis versus skewness plot. The dashed line is the curve fitting of $K = 1.5/S^2 + 2.8$.

mixture fraction show peaks at the vortex shedding frequency as shown in figure 11. Comparing the spectral densities of the velocity and of the mixture fraction shows that at high frequency the spectral density of velocity decreases faster than that of the mixture fraction. Figure 11 shows the spectral densities for the conserved scalar at $x'/M = 0.39$, 0.77 and $1.55 (x_0 = 2.465$ m) at the centre of the plume. The spectral densities of the mixture fraction at $x'/M = 0.39$ and 0.77 have been shifted by one and two decades, respectively, for clarity. It can be seen from the figure that the spectral densities show peaks at the vortex-shedding frequency and its first harmonic at $x'/M = 0.39$. The peaks are very small at $x'/M = 0.77$ and no peak is apparent at $x'/M = 1.55$. This is consistent with the finding of Stapountzis *et al.* (1986), who conclude that the vortex shedding ceases to influence the spectral densities beyond $x'/M \sim 1$.

It can be concluded that in general a conserved scalar determined from the reactive scalars in the turbulent reactive plume shows the same mixing characteristics as a passive scalar in the thermal plume. This is consistent with the conserved scalar theory of Bilger *et al.* (1991) and confirms that small differences in the molecular diffusitivities of the species do not have a significant effect in turbulent mixing. Koochesfahani & Dimotakis (1986) compared the results from a liquid mixing layer of Schmidt number $S_c = 600$ and in a gas phase of $S_c \approx 0.7$ (which is about the same as in the present experiment), and found that the normalized amount of chemical product formed in the liquid layer at high Reynolds number is 50% less than the corresponding quantity measured in the gas-phase case. From this they concluded that Schemit number plays a role in high Reynolds number mixing. The present experiments have a high Reynolds number but the difference in Schmidt number for the different species is small. It could be that any difference in mixing due to the Schmidt number difference is within experimental error. Thus the present conclusion does not contradict that of Koochesfahani & Dimotakis (1986).

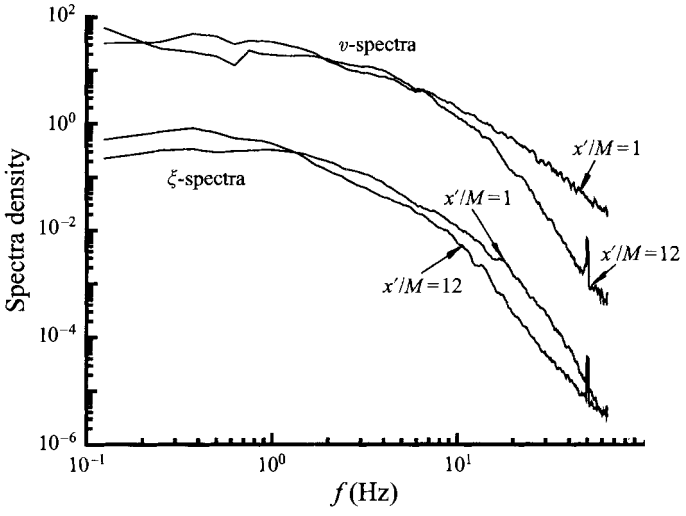

FIGURE 10. Spectral densities of v-velocity and conserved scalar. The v-velocity spectral densities have been multiplied by 100 ($x_0 = 0.424$ m).

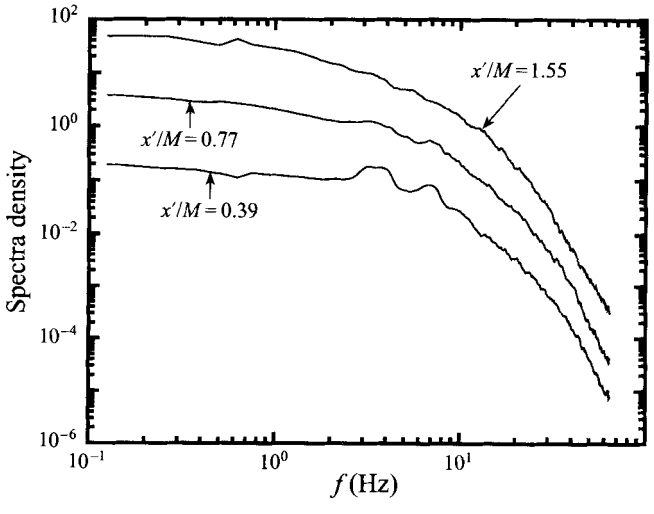

FIGURE 11. Spectral densities for the conserved scalar at different downstream locations and on the centre of the plume. The spectral densities at $x'/M = 0.77$ and 0.55 have been multiplied by 10 and 100, respectively.

3.4. *Reactive scalars*

Bilger *et al.* (1991) present a conserved scalar theory for reactive scalars in turbulent reacting flow. The theory shows that in turbulent reacting flows there are the frozen and equilibrium limits for the species concentrations. The former corresponds to slow chemistry ($N_D = 0$) and the latter to fast chemistry ($N_D \to \infty$). In the frozen and equilibrium limits, the concentrations of the reactive scalars are directly connected to the mixture fraction. In the present system, these relationships are

$$\Gamma^0_{NO} = \xi \Gamma_{NO_1}\,,\ \Gamma^0_{O_3} = (1-\xi)\Gamma_{O_{3_2}}, \tag{3.4}$$

$$\Gamma^e_{NO} = (\Gamma_{NO_1} + \Gamma_{O_{3_2}})(\xi - \xi_s)H(\xi - \xi_s)\,,\ \Gamma^e_{O_3} = (\Gamma_{NO_1} + \Gamma_{O_{3_2}})(\xi_s - \xi)H(\xi_s - \xi) \tag{3.5}$$

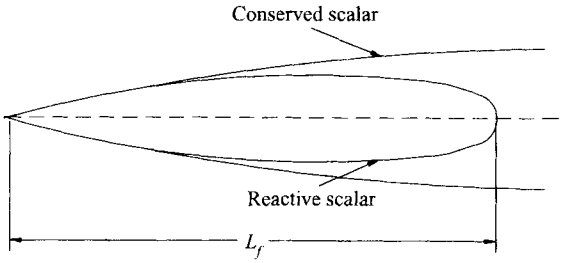

FIGURE 12. Schematic diagram for the spread of the conserved scalar and the plume reactant.

where superscripts 0 and e stand for the frozen and equilibrium limits respectively, and H is the Heaviside function. For details of the conserved scalar theory, refer to Bilger *et al.* (1991), who find that in a turbulent scalar mixing layer, the data of the mean reactant concentrations at finite Damköhler number fall between the frozen and equilibrium limits as they should according to the conserved scalar theory. They also find that the r.m.s. values of the reactant concentrations have a tendency to fall between the frozen and equilibrium limits, although there is no realizability constraint that they should. In presenting the data for reactive scalars, we will compare them with the conserved scalar theory as much as possible. Instead of calculating the frozen and equilibrium limits using the p.d.f. method as suggested in Bilger *et al.* (1991), Γ^0_{NO}, Γ^0_{O3}, Γ^e_{NO}, and $\Gamma^e_{O_3}$ have been calculated directly from the time series data using (3.4) and (3.5), and the various corresponding statistics obtained directly. It is found that both methods agree with each other.

One of the differences between the reactive and non-reactive plumes is that, in the reactive plume, the plume reactant will be completely consumed at a certain downstream position. This situation is similar to that of a turbulent diffusion jet flame. In a diffusion jet flame, a flame length L_f exists. Figure 12 shows a schematic diagram for the spread of the conserved scalar and the plume reactant. In the reactive plume, L_f depends on the stoichiometric mixture fraction ξ_s. The larger ξ_s is, the smaller is L_f. The physical reason for this is that when ξ_s is large, the ratio between the background reactant (O_3) and the plume reactant (NO) is high. The plume reactant will thus be completely reacted with a smaller ingestion of background fluid giving a smaller L_f.

Figure 13 shows the measured mean NO concentration profiles downstream of the line source in both the near and far fields. The data have been normalized by their centreline value $\overline{\Gamma}_{NO_c}$. In the figure the traverse distance y has been normalized by σ_1, the same as that for the conserved scalar. Also shown in the figure is the Gaussian profile. Although the data collapse together and the Gaussian profile fits the data reasonably well, a close look at the figure shows that $\overline{\Gamma}_{NO}/\overline{\Gamma}_{NO_c}$ is in general below the Gaussian curve. The normalized mean O_3 concentration profiles, $(\overline{\Gamma}_{O_{3_2}} - \overline{\Gamma}_{O_3})/(\overline{\Gamma}_{O_{3_2}} - \overline{\Gamma}_{O_{3_c}})$, show similar behaviour to that for $\overline{\Gamma}_{NO}/\overline{\Gamma}_{NO_c}$ except that the data are in general above the Gaussian profile. Figure 14(*a,b*) shows $\overline{\Gamma}_{NO}/\overline{\Gamma}_{NO_c}$ profiles at $N_D = 0$ (frozen limit), finite and ∞ (equilibrium limit) at $x'/x_0 = 6.0$ and 9.0 ($x_0 = 0.425$ m). From the figure it can be seen that the normalized mean $\overline{\Gamma}_{NO}$ profiles have only a very weak dependence on N_D. The normalized $\overline{\Gamma}_{O_3}$ profiles have even weaker N_D dependence than those for $\overline{\Gamma}_{NO}$. Figure 14(*a,b*) shows that the spread rate of the NO species in a turbulent reacting plume is less than that in a non-reactive plume due to chemical reaction. This is because the chemical reaction consumes NO

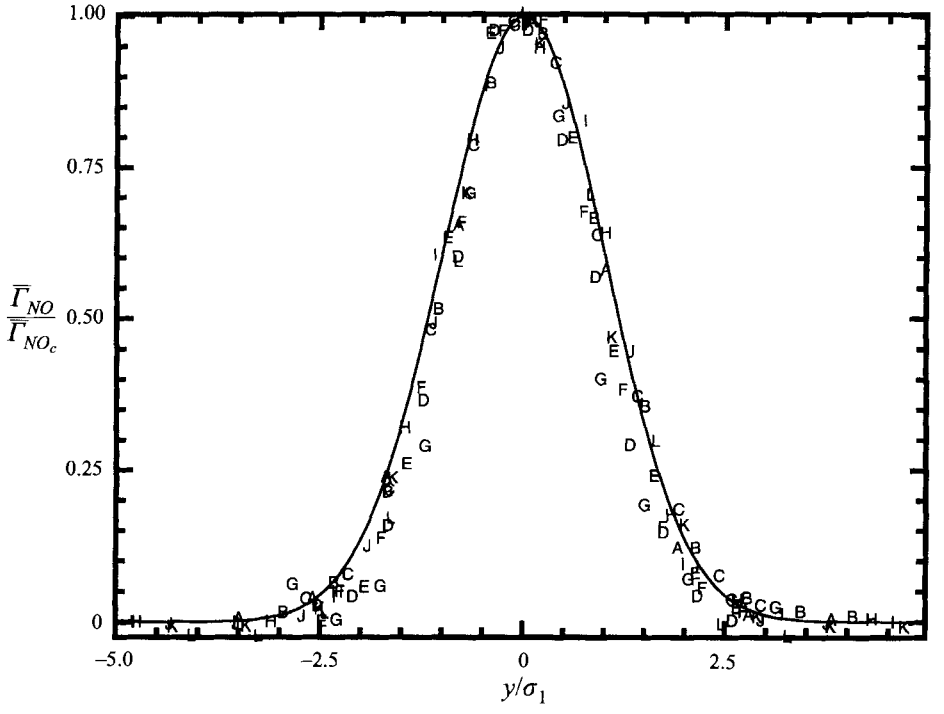

FIGURE 13. The profiles of $\overline{\Gamma}_{NO}/\overline{\Gamma}_{NO_c}$. Symbols are listed in table 1. Solid line is the Gaussian profile.

as it spreads into the ambient O_3-rich air. Comparing figure 14(*a*) and 14(*b*) shows the effect of the stoichiometric mixture fraction: $\xi_s = 0.079$ at $x'/x_0 = 6.0$ (figure 14*a*) and $\xi_s = 0.045$ at $x'/x_0 = 9.0$ (figure 14*b*). With a 75% difference in ξ_s, the difference in the width of the reactive plume (relative to that of the conserved plume) is only 5%, which can be considered to be small. This is also consistent with the results shown in figure 13, where the width of the reactive plume has only a small spread although the Damköhler numbers are different at different stations and the stoichiometric mixture fraction ξ_s varies from 0.045 to 0.134. Thus it can be concluded that the present experiments have been conducted mainly within $x'/L_f < 1$. Within this range the effect of chemical reaction on the lateral spread of the plume is small, and the spread of the plume is mainly due to the turbulent mixing.

Figure 15 shows the downstream development of the centreline values of the mean NO concentration for the non-reactive plumes and the reactive plumes at finite and fast chemistry. In presenting the results for the fast chemistry, those at $(\xi_s)_{max}$ and $(\xi_s)_{min}$ have been calculated from the equilibrium limit given in Bilger *et al.* (1991), which is

$$\overline{\Gamma^e_{NO}} = (\Gamma_{NO_1} + \Gamma_{O_{3_2}})\{(\overline{\xi} - \xi_s)H(\overline{\xi} - \xi_s) + J_1\xi'\}.$$

The J_1 in the above expression is given by Mudford & Bilger (1985) as

$$J_1 \approx 0.45\exp\{-|\overline{\xi} - \xi_s|/\xi'\}.$$

$\overline{\Gamma^e}_{NO}$ can also be obtained using (3.5) directly for different ξ_s.

In figure 15 the mismatch of the normalized NO concentrations for $N_D = 0$ at $x'/x_0 \approx 0.8$ can be attributed to the facts that: (i) l_0 is different for the measurements taken in the near field and those in the far field; and (ii) the correction to the plume

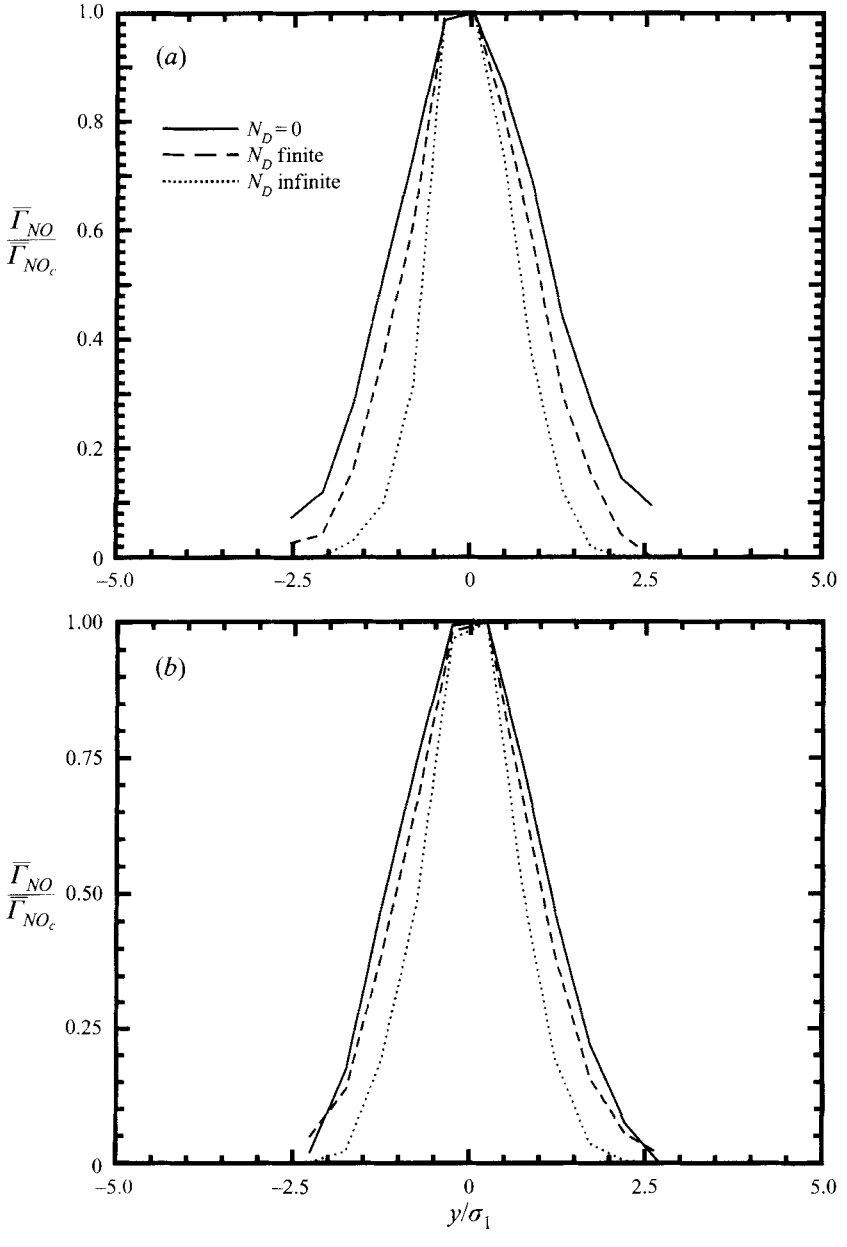

FIGURE 14. Normalized mean reactive scalars $\Gamma_{NO}/\Gamma_{NO_e}$, at different N_D. (*a*) $x'/x_0 = 6.0$, $\xi_s = 0.079$, $\bar{\xi} = 0.068$; (*b*) $\Gamma_{NO}/\Gamma_{NO_e}$, $x'/x_0 = 9.0$, $\xi_s = 0.045$, $\bar{\xi} = 0.0563$.

spread rate σ_1 from σ_0 will have a larger effect in the near field than that in the far field. The conservation of NO species in the non-reactive plume requires $\sigma_1 \overline{\Gamma}_{NO_e} = \text{const.}$ (equation (3.1)). Using this and figure 3 it can be shown that $l_0 \overline{\Gamma}_{NO_e}/\Gamma_{NO_1} \propto 1/(\sigma_1/l_0)$. Figure 15 shows that the centreline mean value of Γ_{NO} at finite N_D falls between the frozen and equilibrium limits. Figure 15 also shows that the chemical reaction has a large effect on the decay of the mean NO concentration. This effect depends strongly on the Damköhler number and the stoichiometric mixture fraction. For the near-field

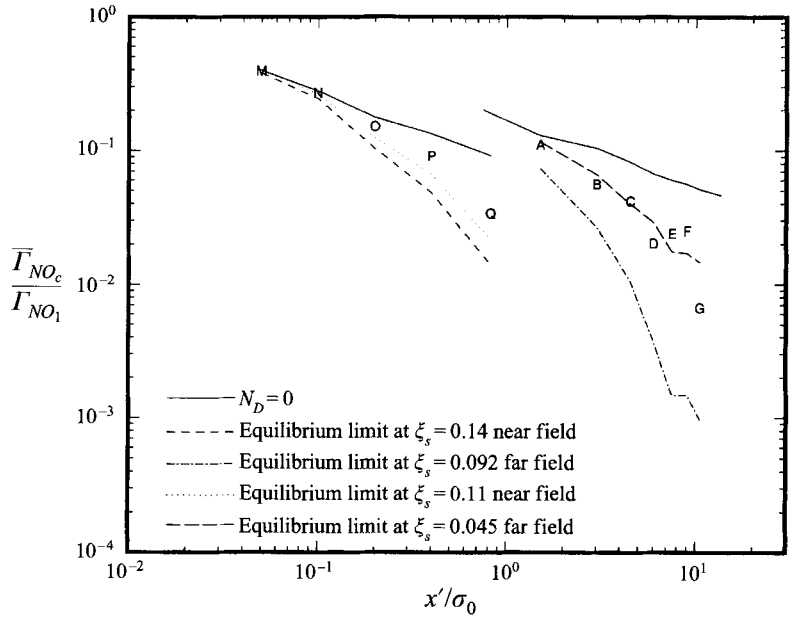

FIGURE 15. Downstream development of the centreline values of mean NO concentration.

experiment, at $x'/x_0 = 0.82$, the mean NO concentration in the reactive plume is only about one third of that in the non-reactive plume. In the far-field experiment, at $x'/x_0 \approx 10$, the mean NO concentration from the reactive plume is less than 15% of that in the non-reactive plume. The mean NO concentrations at the equilibrium limits are even less. Also figure 15 shows that the effect of the chemical reaction on the decay of the mean NO concentration depends on the travelling time (or the absolute distance) of the reactive species from the line source to the measuring station rather than on the normalized time t'/t_0. This can be seen if we shift the results of the far field down so that the results of the frozen limit in the near and far fields match at around $x'/x_0 = 0.8$. If the decay of mean NO concentration did depend on the relative time t/t_0, we would expect that point A in figure 15 would match point Q which is at $x'/x_0 = 0.8$.

In order to check the effect of the stoichiometric mixture fraction ξ_s on the decay of the plume reactant, let us have a close look at $\overline{\Gamma}_{NO_c}/\Gamma_{NO_1}$ at $x'/x_0 = 6.0$ (symbol D in figure 15) and 9.0 (symbol F in figure 15) in the far field: $\xi_s = 0.045$ at $x'/x_0 = 9.0$ and $\xi_s = 0.079$ at $x'/x_0 = 6.0$. At $x'/x_0 = 6.0$ figure 15 shows that $\overline{\Gamma}_{NO_c}/\Gamma^0_{NO_1} = 0.3$. By extrapolation, it can be estimated that at $\xi_s = 0.079$, $\overline{\Gamma}_{NO_c}/\Gamma^0_{NO_1}$ should be about 0.16 at $x'/x_0 = 9.0$. The experimental data give $\overline{\Gamma}_{NO_c}/\Gamma_{NO_1} = 0.43$ at $\xi_s = 0.045$, a factor of 3 different to $\overline{\Gamma}_{NO_c}/\Gamma_{NO_1} = 0.16$ at $x'/x_0 = 9.0$. This is in contrast with a 5% difference between the width of the reactive plume and that of the non-reactive plume at the same stoichiometric mixture fraction difference as mentioned earlier.

Figure 16(*a,b*) shows the profiles of γ'_{NO} and γ'_{O_3}, the r.m.s. values of the Γ_{NO} and Γ_{O_3} concentration fluctuations. The data have been normalized by the centreline values and the cross-stream coordinate y has been normalized by σ_1. In comparison with the r.m.s. profiles for the conserved scalar, the γ'_{NO} has only one peak occurring at the centre of the plume and γ'_{O_3} has the off-centre peaks in both the near and far fields. The normalized r.m.s. profiles of NO concentration seem to collapse together

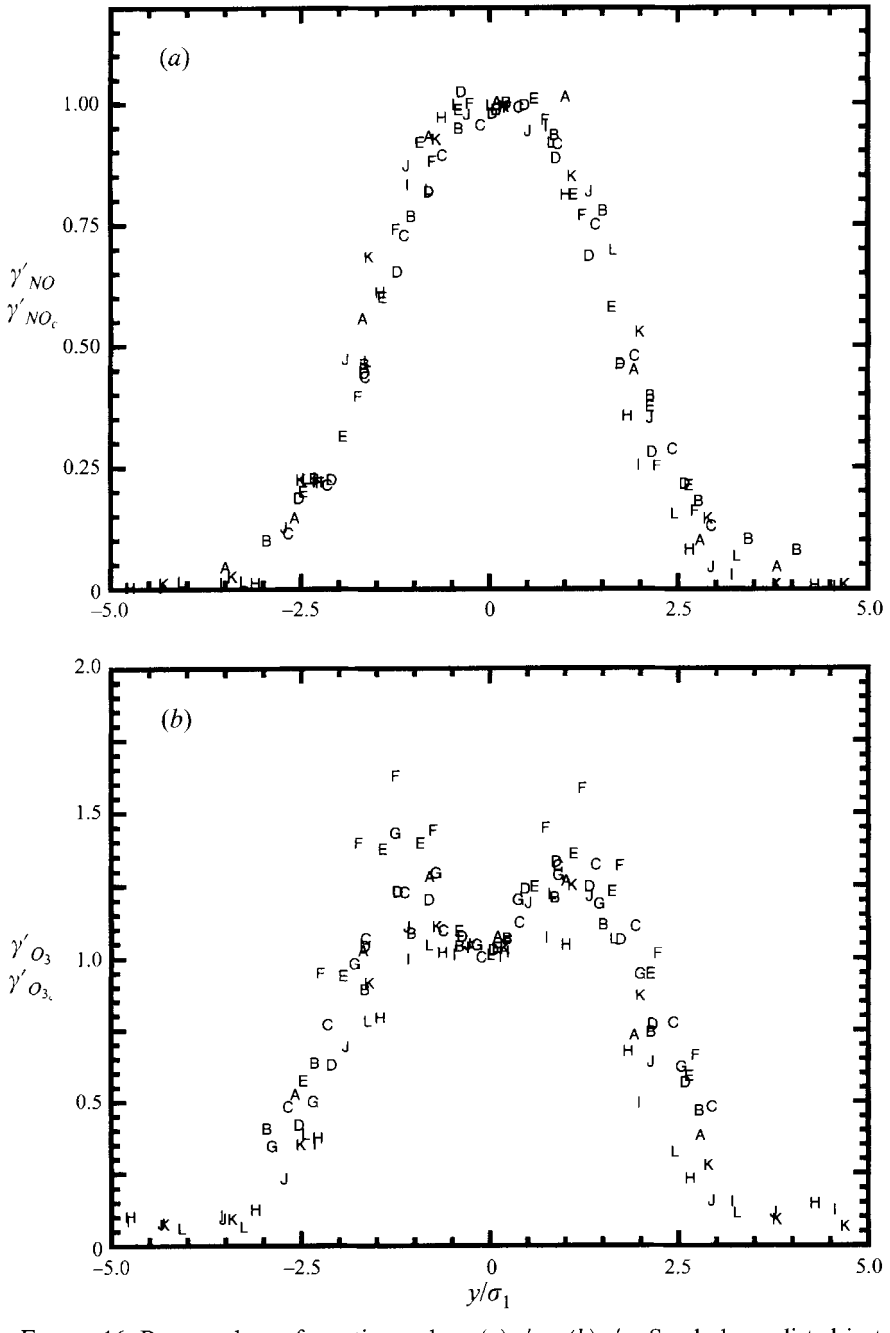

FIGURE 16. R.m.s. values of reactive scalars. (*a*) γ'_{NO}; (*b*) γ'_{O_3}. Symbols are listed in table 1.

and can be represented by a single curve but those for the O_3 concentration cannot be represented by a single curve because the normalized peak values vary with x'/x_0. Figures 17(*a*,*b*) compares the r.m.s. profiles of the reactive scalar at $x'/x_0 = 7.5$ ($x_0 = 0.425$ m) with that of the frozen and equilibrium limits. The figures show that the γ'_{NO} profiles change from a single peak at the centre of the plume at the equilibrium limit to double peaks at the frozen limit. The results at $N_D = 5.4$ fall

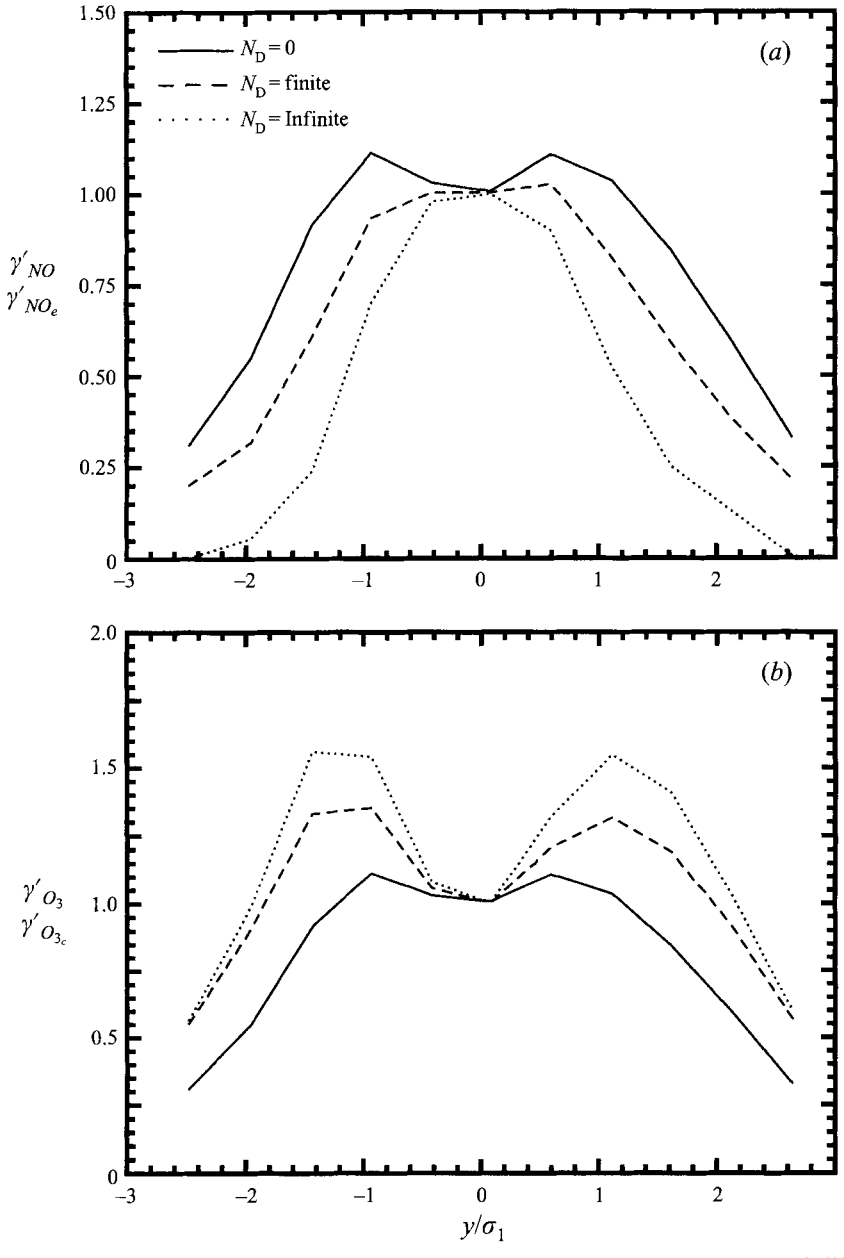

FIGURE 17. R.m.s. values of reactive scalar at $x'/x_0 = 7.5$ ($x_0 = 0.425$ m) and different N_D. (*a*) $\gamma'_{NO}/\gamma'_{NO_e}$; (*b*) $\gamma'_{O_3}/\gamma'_{O_{3e}}$.

between the two limits and have a flat region at the centre. However the γ'_{O_3} profiles show double peaks for both the frozen and equilibrium limits. In the frozen limit, equation (3.4) shows that in the downstream development of the plume the intensities of the Γ_{NO} and Γ_{O_3} fluctuations will have behaviour similar to that of the mixture fraction fluctuations.

Figure 18(*a*,*b*) shows the centreline values of γ'_{NO} and γ'_{O_3} at finite chemistry and at the frozen and equilibrium limits. The data have been normalized by Γ_{NO_1} and $\Gamma_{O_{3_2}}$,

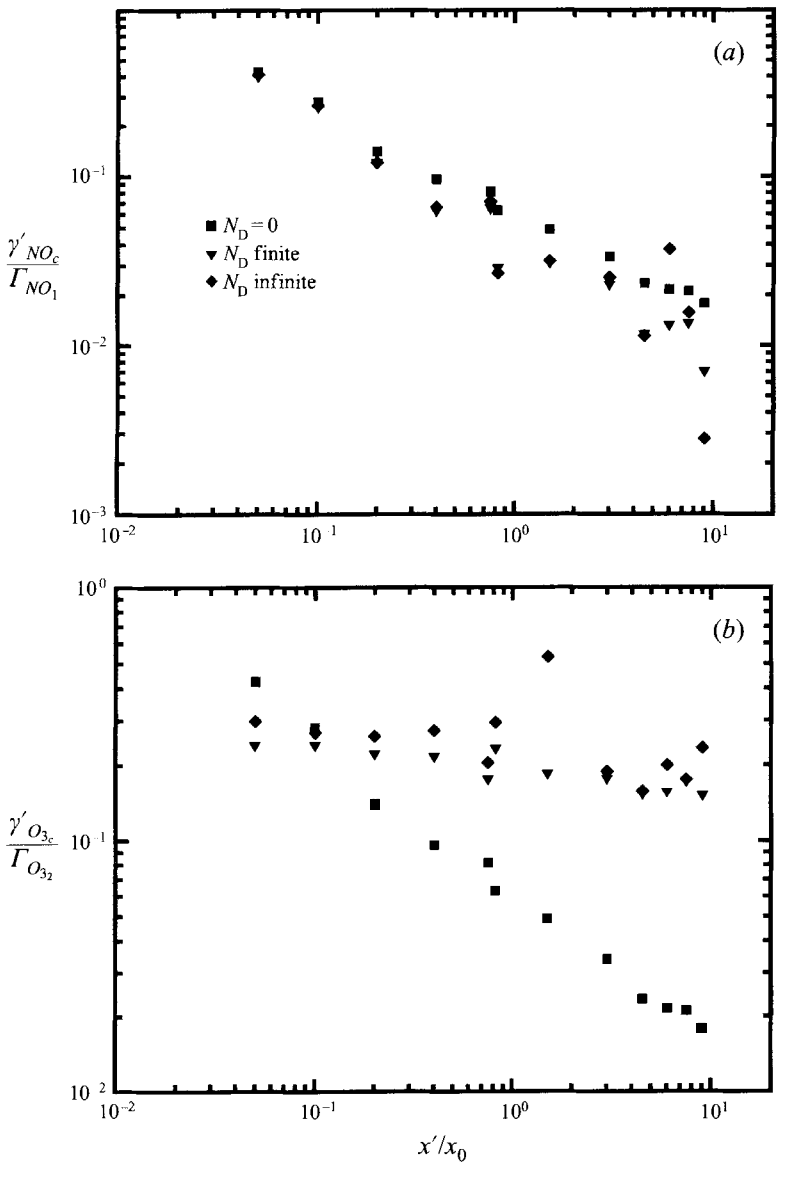

FIGURE 18. The centreline values of γ'_{NO} and γ'_{O_3}. (*a*) $\gamma'_{NO}/\Gamma_{NO_1}$; (*b*) $\gamma'_{O_3}/\Gamma_{O_{3_2}}$.

respectively. It can be seen that $\gamma'_{NO}/\Gamma_{NO_1}$ decreases with increasing x'/x_0, and the γ'_{NO} values at the frozen limit are in general the largest among the three N_D values. In general the γ'_{NO} values at N_D = finite (≈ 5.4) and ∞ are about the same. Comparing figure 18(*a*) with figure 17(*a*) shows that γ'_{NO} values away from the centre of the plume at finite Damköhler number in general fall between those of the frozen and equilibrium limits. Figure 18(*b*) shows that although the centreline value of $\gamma'_{O_3}/\Gamma_{O_{3_2}}$ decays rapidly with increasing x'/x_0 at $N_D = 0$, those for N_D = finite and ∞ decay much more slowly. Again the γ'_{O_3} values at N_D = finite and ∞ are about the same.

This behaviour of $\gamma'_{NO_c}/\Gamma_{NO_1}$ and $\gamma'_{O_{3_c}}/\Gamma_{O_{3_2}}$ can be explained as follows. In both the reactive and passive plumes, the mean NO concentration decreases as x'/x_0 increases.

Because of this the maximum Γ_{NO} will decrease while the minimum Γ_{NO} will be close to zero in the centre of the plume when $N_D \neq 0$. Thus the range of Γ_{NO} fluctuations will decrease as x'/x_0 increases. This will reduce γ'_{NOc} and the rate of its decay will be similar to that for Γ_{NO_c}. The γ'_c/Γ_{NO_c} values (not shown here) are indeed close to being constant, thus supporting the above argument. In the turbulent reactive plume the maximum Γ_{O_3} will always be $\Gamma_{O_{3_2}}$ while the minimum Γ_{O_3} will be zero (unless the NO species has been almost completely reacted). Thus the range of Γ_{O_3} fluctuation will be almost the same during the downstream development of the plume. Because of this the $\gamma'_{O_{3c}}$ values will be almost be constant. The behaviour of $\gamma'_{O_{3c}}/\Gamma_{O_{3_2}}$ at the frozen limit is due to the fact that at the centre of the plume the mixing of the two non-reactive scalars will increase the minimum concentration of O_3, and this reduces the corresponding fluctuation ranges for Γ_{O_3} because $\Gamma_{O_{3_2}}$ is constant. The behaviour of $\gamma'_{NO}/\Gamma_{NO_1}$ at the frozen limit is due to the fact that the mean NO concentration at the centre of the plume decreases more slowly at the frozen limit than that for the finite-rate chemistry. This results in a larger fluctuation range for the NO concentration at the frozen limit than for finite-rate chemistry, and hence results in slightly higher r.m.s. values of the NO concentration at the frozen limit than for finite-rate chemistry.

Combining figures 18(*b*) and 17(*b*) shows that in general the γ'_{O_3} values at finite Damköhler number fall between those at the frozen and equilibrium limits with those at the equilibrium limit having the highest values. Theoretically there is no constraint that γ'_{NO} and γ'_{O_3} should fall between the frozen and equilibrium limits, although the data of Bilger *et al.* (1991) in a scalar mixing layer show that both intensities tend to fall between these limiting cases. The present experimental data in the turbulent reactive plume are consistent with those of Bilger *et al.* (1991).

Figure 19 shows the correlation coefficient of NO and O_3 concentration fluctuations. Also shown in the figure are the results at the equilibrium limit at $x'/x_0 = 3.0$ ($x_0 = 0.425$). Within $-2 < y/\sigma_1 < 2$, the data show a constant of -0.86 for all the downstream positions. This is lower than that of Bilger *et al.* (1991) in the scalar mixing layer (their results are between -0.8 and -0.6). At the centre of the plume the correlation coefficient at the equilibrium limit is about -0.5, which is about the same as that of Bilger *et al.* (1991). The corresponding value at the frozen limit is -1 (Bilger *et al.* 1991), and it can be seen that in general the data fall between the frozen and equilibrium limits. From the scalar mixing layer data, Bilger *et al.* (1991) conclude that both the closure models of Toor (1969) and Mudford & Bilger (1985) disagree with their experimental data for the correlation of the two reactive scalars. A similar conclusion applies here. The data in figure 19 suggest that in the centre region of the plume the relationship

$$\overline{\gamma_{NO}\gamma_{O_3}} = \alpha\gamma'_{NO}\gamma'_{O_3} \tag{3.6}$$

models the data well. However, given the fact that $\alpha = -1$ in the frozen limit and $\alpha \approx -0.5$ in the equilibrium limit, it is clear that $\alpha = \alpha(N_D)$. Also it is believed that α depends on the flow conditions as well.

3.5. *The turbulent flux*

Figure 20 shows the profiles of the correlation coefficient between the traverse velocity v and the conserved scalar ξ. The correlation coefficient between v and Γ_{NO} is similar to that for v and ξ, and that between v and Γ_{O_3} is of opposite sign to that for v and ξ (not shown here). The anti-symmetrical behaviour of the data is clearly shown in the figure.

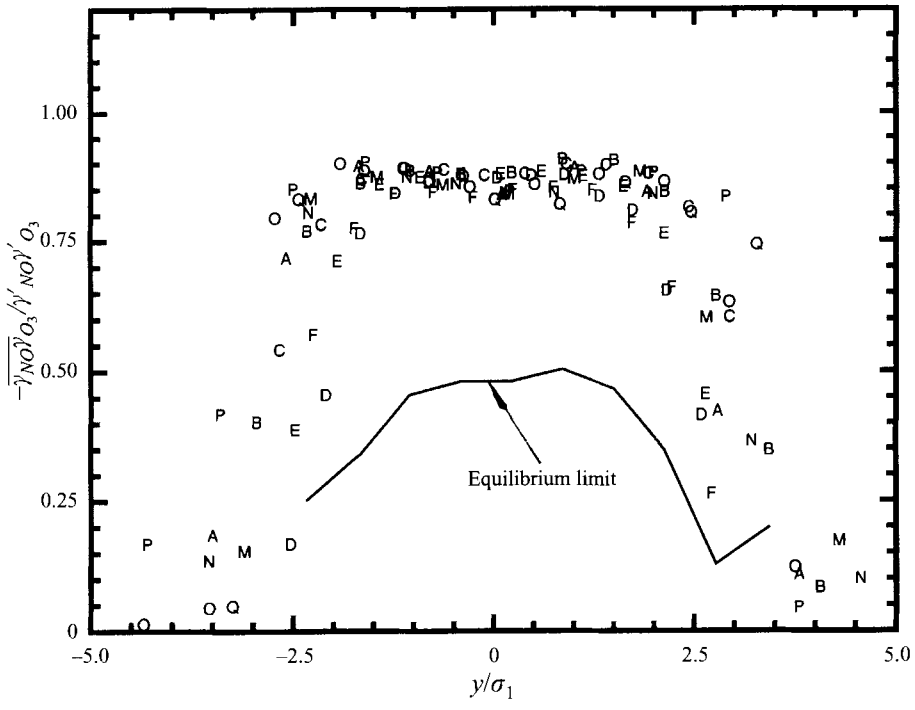

FIGURE 19. Correlation coefficient of NO and O_3 concentration fluctuations. Symbols are listed in table 1.

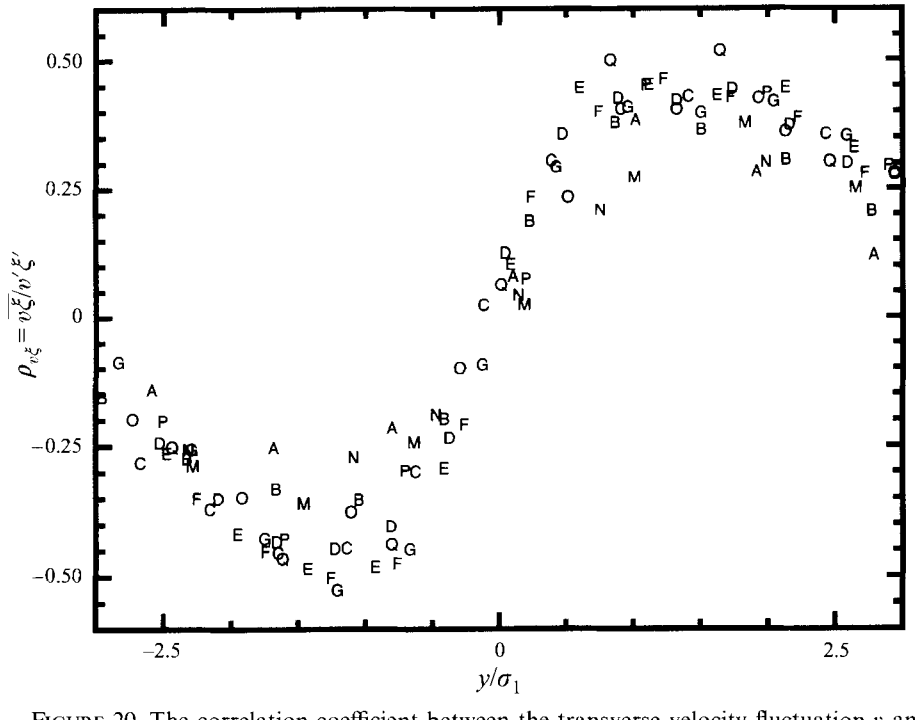

FIGURE 20. The correlation coefficient between the transverse velocity fluctuation v and the conserved scalar, $\rho_{v\xi} = \overline{v\xi}/v'\xi'$.

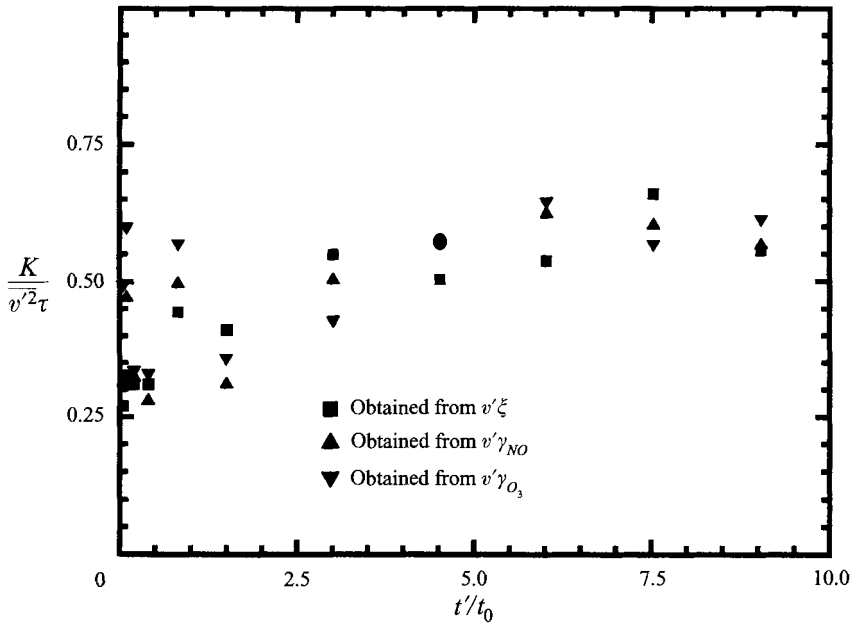

FIGURE 21. Turbulent diffusitivity deduced from the conserved and reactive scalars.

One of the difficulties in modelling turbulent plumes behind line sources is that the gradient model fails to give satisfactory results. The physical reason for this is that the integral length scale for scalars is smaller than that for turbulence (Corrsin 1974), especially at a distance not too far away from the source. The usual model for the turbulent flux is

$$\overline{v'\xi'} = -K\frac{\partial\overline{\xi}}{\partial y} \tag{3.7}$$

where K is the turbulent diffusitivity. Using $K = \frac{1}{2}\mathrm{d}\sigma_1^2/\mathrm{d}t$ (Deardorff 1978; Anand & Pope 1985) and σ_1^2 given by Anand & Pope (1985), it can be shown that for a line source in a homogeneous decaying turbulent flow field

$$K = \beta\overline{v'^2}\tau\{1-(1+t/t_0)^{-\frac{1}{2}m(\frac{3}{2}C_0-1)-1}\} \tag{3.8}$$

where β is a constant, τ the integral time scale of turbulence, $t = x'/U$, $t_0 = x_0/U$, m the energy decay exponent and C_0 is a constant. The important thing to note about (3.8) is that unless $t \gg t_0$, the non-dimensional turbulent diffusitivity, $K/\overline{v'^2}\tau$ depends on t rather than being a constant as the gradient model requires.

Bilger *et al.* (1991) find that the turbulent diffusitivity deduced from the reactive scalars is substantially higher than that deduced from the mixture fraction on the side of the scalar mixing layer from where the reactive scalars come, but is much lower on the other side of the scalar mixing layer. Toor (1993) proposes a theory to explain this difference. However in the present line source experiment, no such difference in turbulent diffusitivities deduced from both the conserved and reactive scalars has been found. Figure 21 shows the turbulent diffusitivity in the centre of the plume calculated using (3.7) for the conserved and reactive scalars based on the present experimental data at different distances from the line source. In figure 21 the time scale τ has been estimated as $\tau = k/\epsilon$. In calculating the turbulent diffusitivity, the mean scalar profiles have been smoothed by curve fitting before differentiation and the data in the region

$-2 < y/\sigma_1 < 2$ have been used to calculate the averaged value. In the figure the data have been presented against t'/t_0. The overall experimental uncertainty for K is about 20%. The result at $t'/t_0 = 0.05$ could be due to the fact that the measurement was taken with $x'/M < 1$ but the high value of K at $t'/t_0 = 0.82$ cannot be explained. It can be seen that in general the turbulent diffusitivities calculated from the conserved and reactive scalars are about the same. This shows that the molecular diffusitivity and the chemical reaction have only a weak effect on the turbulent diffusitivity. Figure 21 shows that $K/\overline{v'^2}\tau$ increases with t'/t_0 when it is small and approaches a constant $\beta \approx 0.6$ when it is large. This is slightly larger than $\beta = 0.5$ given by Deardorff & Wills (1975) for a convective mixed boundary layer, and smaller than $\beta = 0.8$ given by Fackrell & Robins (1982) in plumes from point sources in a neutral turbulent boundary layer. Deardorff (1978) shows that in a turbulent plume, when the first-order gradient modelling fails, it is likely that the second- and third-order gradient modelling will also fail. Because of this we would expect that the gradient model of the first, second and third order will not work well for both the passive and reactive scalars in $t'/t_0 < 5$. However figure 21 shows that the gradient model, at least to the first order, should work well for $t'/t_0 > 5$ in the present plume.

3.6. *The conserved scalar dissipation*

The second difficulty in modelling the turbulent plume behind a line source is to model the scalar dissipation rate correctly. The commonly used model is

$$\epsilon_\xi = C_\xi \overline{\xi'^2}/\tau \tag{3.9}$$

where $\epsilon_\xi = 2D\overline{(\partial\xi/\partial x_i)^2}$, D is the molecular diffusitivity, C_ξ is a constant and a value of $C_\xi = 2$ is usually employed (e.g. Anand & Pope 1985). It is known that this model is not correct in general, and particularly in the near fields of plumes. As the plume reactant leaves the line source, the small scale which characterizes the scalar field in the plume is correlated with the size of the line source. As the plume develops the small scale of the turbulence will become more and more important and that of the line source less and less so. The constant $C_\xi = 2$ will apply only when the effect from the length scale of the line source is negligible.

By invoking local isotropy and Taylor's frozen flow hypothesis, the scalar dissipation can be calculated according to

$$\epsilon_\xi = 6D\overline{(\partial\xi/\partial t)^2}/U^2. \tag{3.10}$$

In this paper only the scalar dissipation measured in the near field will be presented since in the far field the frequency response of the CLA I is not high enough to resolve all the small-scale fluctuations which contribute to the scalar dissipation. In order to be confident that CLA II can capture most of the scalar dissipation in the near-field measurements, the following checks have been performed.

(*a*) The Kolmogorov length scale for the present near-field experiment varies from 1.54 mm at $x'/x_0 = 0.05$ to 2.32 mm at $x'/x_0 = 0.82$. Using Taylor's hypothesis this corresponds to 325 Hz and 216 Hz respectively. Based on the experimental data of Warhaft & Lumley (1978), Veeravalli & Warhaft (1990) conclude that the maximum passive scalar dissipation occurs at the length scale of about 30η and has a negligible contribution from scales smaller than 6η. This means that the maximum scalar dissipation in the present experiment would occur at about 11 Hz and 7 Hz, respectively. The present variance dissipation spectral densities confirm this conclusion.

(*b*) The data of Warhaft & Lumley (1978) show that the contribution to the scalar

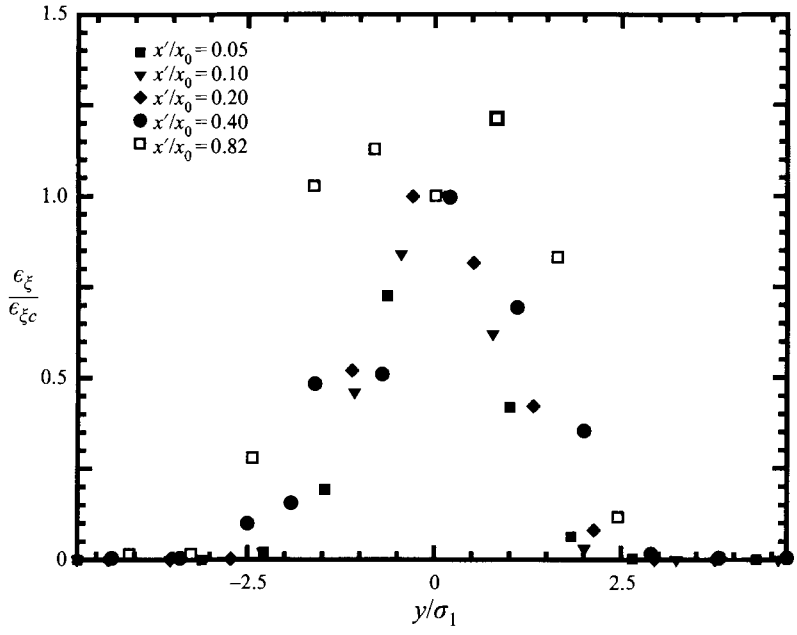

FIGURE 22. The dissipation of conserved scalar (normalized by the centreline values), $\epsilon_\xi/\epsilon_{\xi_c}$.

dissipation from scales smaller than 12η is less than 10% (at $S_c \approx 0.7$). The CLA based on the photon-counting technique has a frequency response of 50 Hz. This is about 6.5η and 4.3η at $x'/x_0 = 0.05$ and 2.32 respectively, after using Taylor's hypothesis.

(*c*) The scalar dissipation can also be equivalently calculated from the one-dimensional variance spectrum $E_\xi(k_1)$ as

$$\epsilon_\xi = 6D \int_0^\infty k_1^2 E_\xi(k_1) \mathrm{d}k_1 \tag{3.11}$$

where k_1 is the one-dimensional wavenumber. In calculating the scalar dissipation from (3.10) and (3.11), it is found that the scalar dissipation calculated using (3.11) is 10% higher than that of using (3.10) at $x'/x_0 = 0.05$ and 2% higher at $x'/x_0 = 0.82$. In the scalar dissipation results presented below, only those calculated from (3.10) are given although Veeravalli & Warhaft (1990) suggest that the spectral method is more accurate. Calculating the scalar dissipation using (3.10) will give more information such as the correlation between the scalar dissipation and the scalar itself (see later).

(*d*) On the centreline of the plume the equation for the conserved scalar variance is

$$U\frac{\partial \overline{\xi'^2}}{\partial x} + 2\overline{u'\xi'}\frac{\partial \overline{\xi}}{\partial x} + \frac{\partial \overline{v'\xi'^2}}{\partial y} = -\epsilon_\xi. \tag{3.12}$$

This has been checked at $x'/x_0 = 0.1$. It is found that the left-hand-side of (3.12) agrees with the right-hand-side to within 5%. Also it is found that in (3.12) the convection of the scalar variance, i.e. the first term dominates the left-hand side while the second term is negligible.

Figure 22 shows the mean conserved scalar dissipation normalized by the centreline values in the near field of the plume. The r.m.s. profiles of the conserved scalar dissipation have a similar shape to those for mean dissipation. The data show a single

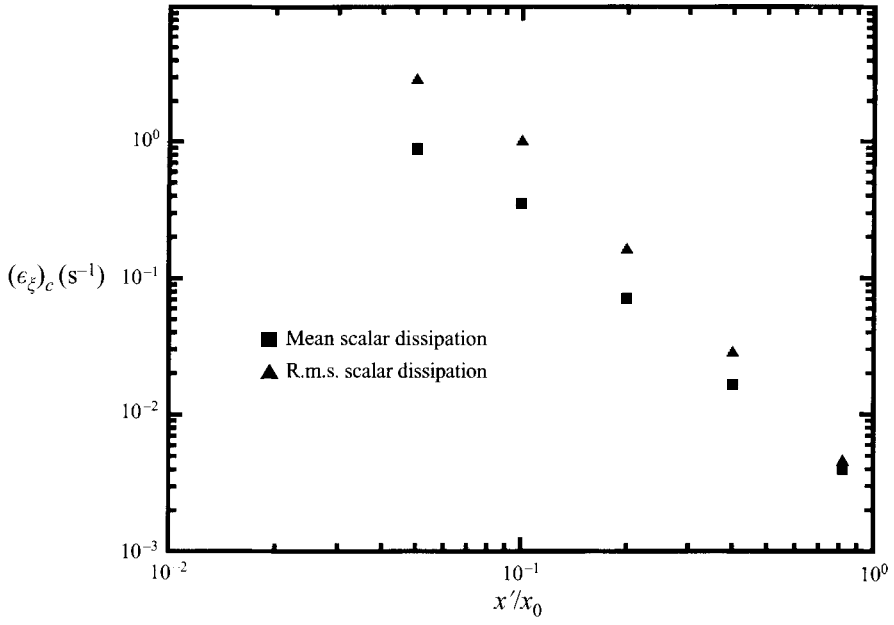

FIGURE 23. The centreline values of the conserved scalar dissipation.

peak at the centre of the plume from $x'/x_0 = 0.05$ to 0.40 and double peaks off the centre of the plume at $x'/x_0 = 0.82$. The appearance of the double peaks in the profiles means that the maximum scalar dissipation moves from the centre of the plume where the local mean profile has a zero gradient to where the maximum gradient occurs in the mean profiles. Figure 23 shows the centreline values of the mean conserved scalar dissipation and its r.m.s. values. The data show that the r.m.s. values are higher than the mean. This is because the p.d.f. of the scalar dissipation is skewed towards the large scalar dissipation fluctuations due to the strongly intermittent characteristics of the small scales. The ratio $\epsilon'_{\xi C}/\epsilon_{\xi C}$ decreases as x'/x_0 increases, with a value of 3.2 at $x'/x_0 = 0.05$ and 1.2 at $x'/x_0 = 0.82$. This indicates that the conserved scalar fluctuations become less intermittent as the plume develops downstream. Immediately after the line source, the gradient of the conserved scalar at the interface between the fluid that carries the conserved scalar and the fluid that does not is close to a delta function, and makes a major contribution to the overall scalar dissipation. During the downstream development of the plume the molecular diffusitivity and turbulent mixing will affect the gradient of the conserved scalar at the interface. Because of this the contribution to the overall scalar dissipation from the interface will become less and less as the plume develops downstream of the line source and the contribution to the scalar dissipation from the small-scale turbulence will become more and more important. Also since the energy decay exponent $n < -1$, the Reynolds number based on Taylor's microscale decreases with increasing x. It is generally accepted that the intermittency of the small-scale turbulence decreases with decreasing Reynolds number. Thus both factors (broadening of the interface and decreasing Reynolds number) will reduce the intermittency of the scalar fluctuations at the small scales as the plume develops downstream of the line source.

The correlation coefficient $\rho_{\xi\epsilon}$ between the conserved scalar and its dissipation in the near field of the plume shows that the correlation is very strong at $x'/x_0 = 0.05$

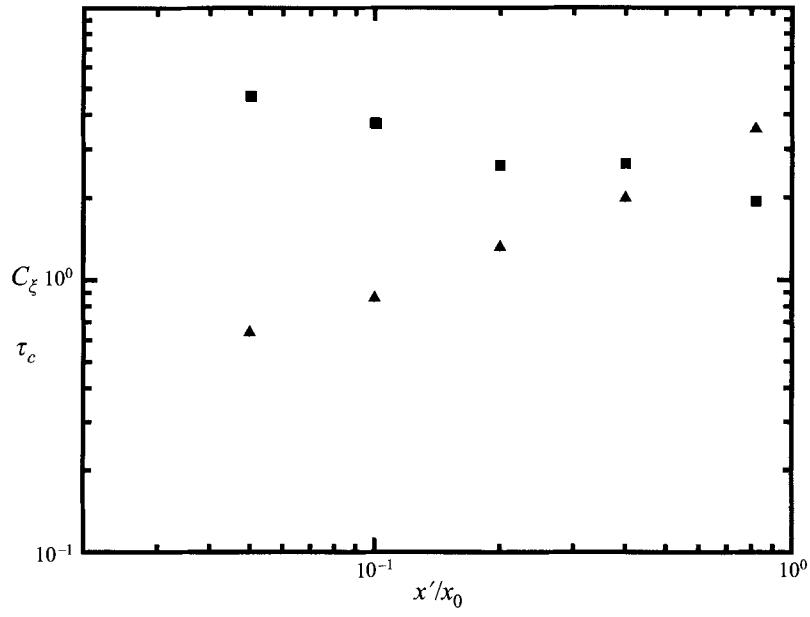

FIGURE 24. The time scale for scalar dissipation τ_c (▲) and the ratio C_ξ (■) between the time scale for energy dissipation and that for the scalar dissipation.

($\rho_{\xi\epsilon} > 0.5$) and weak at $x'/x_0 = 0.82$ ($\rho_{\xi\epsilon} \approx 0$ at the centre of the plume). Figure 24 shows the time scale of the scalar dissipation $\tau_c = \xi'^2/\epsilon_\xi$ and C_ξ, which is the ratio between the time scale of the energy dissipation and that of scalar dissipation. It can be seen that τ_c increases with x'/x_0 and C_ξ decreases with x'/x_0. C_ξ approaches a value of 2, which is the generally used value in modelling the scalar dissipation. Figure 24 shows that at $x'/x_0 = 0.05$, $C_\xi \approx 5$. This value should also depend on the size of the line source and it is considered that as x'/x_0 decreases C_ξ would be even higher. Because at a fixed x'/x_0, C_ξ depends on the size of the line source, it is possible that the distance within which $C_\xi \to 2$ will also depend on the size of the line source. This needs to be investigated further.

3.7. *Mean reaction rates*

Figure 25(*a*,*b*) shows the mean chemical reaction rate $\widetilde{\dot{w}} = -\overline{\dot{w}_{NO}}/\kappa\Gamma_{NO_1}\Gamma_{O_{3_2}} = \overline{\Gamma_{NO}\Gamma_{O_3}}/\Gamma_{NO_1}\Gamma_{O_{3_2}}$ at $x'/x_0 = 0.05$ (near field) and 9.0 (far field), respectively. Also shown in the figure are the different models for the mean chemical reaction rate. These include the closure which uses the product of the mean concentrations and Toor's (1969) closure which sets the covariance $\overline{\gamma_{NO}\gamma_{O_3}}$ equal to its equilibrium value $\overline{\gamma^e_{NO}\gamma^e_{O_3}}$. It is clear from the figures that the product of the means drastically overestimates the mean chemical reaction rate in both the near and far field of the plume and Toor's (1969) closure in general overestimates the mean chemical reaction rate by about 20% in the centre region of the plume. Also shown in the figure are the results which model the mean chemical reaction rate using the frozen limit, i.e. sets the covariance $\overline{\gamma_{NO}\gamma_{O_3}}$ equal to its frozen value $\overline{\gamma^0_{NO}\gamma^0_{O_3}}$. The model underestimates the chemical reaction rate by less than 10% in both the near and far fields. Thus this model is closer to the experimental data than Toor's (1969) closure. This can be explained by using figure 19, which shows that the correlation coefficient between the two reactive scalars is about −0.85 in the centre of the plume while that at the

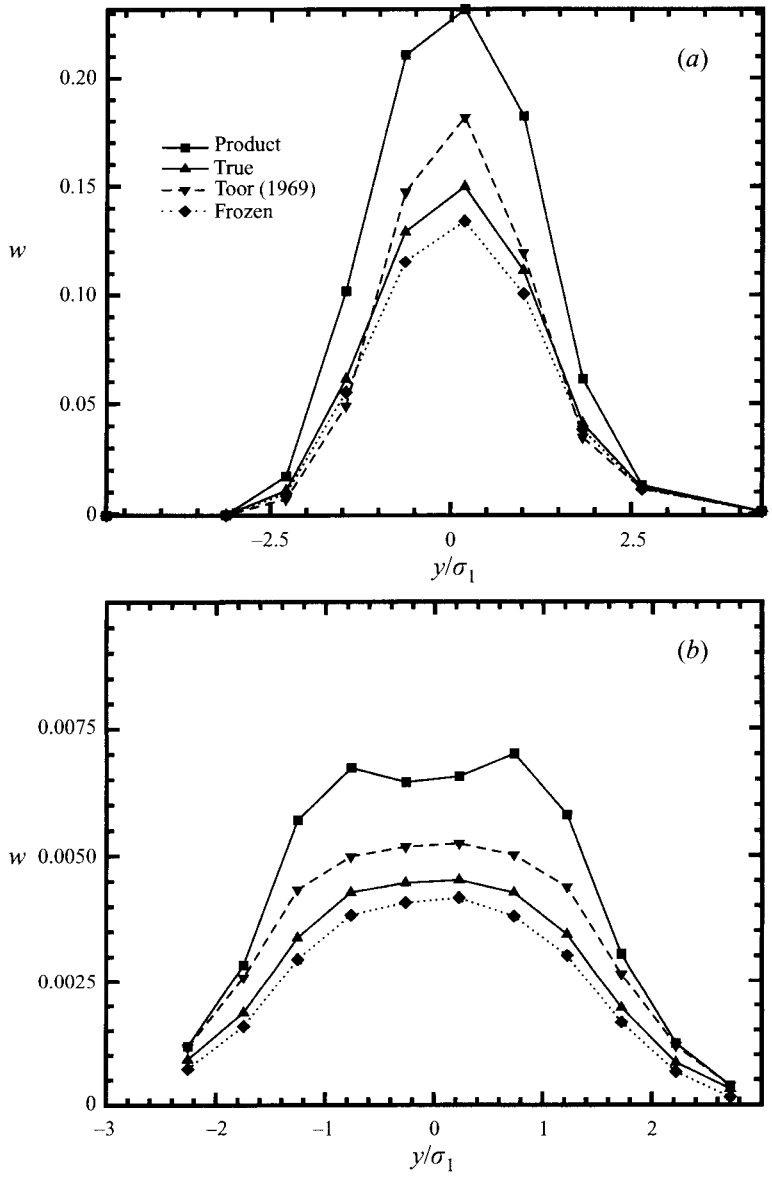

FIGURE 25. The normalized mean chemical reaction rate. (*a*) $x'/x_0 = 0.05$ ($x_0 = 2.465$ m), near field; (*b*) $x'/x_0 = 9.0$ ($x_0 = 0.425$ m), far field.

frozen limit is −1 and that at the equilibrium limits is −0.5. Figure 25(*a,b*) suggests that at finite Damköhler number, modelling the mean chemical reaction rate using an interpolation between the frozen and equilibrium limits for the covariance of the two reactive scalars may be more appropriate.

4. Conclusions

Experimental results for the conserved and reactive scalars in reactive plumes behind a line source have been presented. The experiments have been conducted in both the near and far fields of the plumes. The working section of the TSC is about

8 m long and the experiment can only be performed within $x/M < 25$. Because of this the experiments on the far field have been conducted by putting the line source in the transition region of the grid turbulence. Results for the conserved scalar in the near and far fields are consistent with the experimental results in the literature for a thermal line source. This supports the reactive scalar results. This is so because the governing equations and the boundary conditions for the non-reactive passive scalar downstream of the thermal line source and those for the conserved scalar downstream of the reactive line source at low heat release environment are the same; the statistics for both scalars should also be the same. Further experimental work is needed using different sizes of the line source and having the line source at a greater distance from the grid.

The experimental data for reactive scalars show that the chemical reaction has only a limited effect on the spread rate of the plume but its effect on the decay of the mean plume reactant concentration (Γ_{NO}) is strong, and depends on the stoichiometric mixture fraction ξ_s and the Damköhler number. The mean concentrations of the reactive scalars in the plume at finite Damköhler number fall between the frozen and equilibrium limits, and this supports the conserved scalar theory of Bilger *et al.* (1991). The r.m.s. profiles for the conserved scalar have a single peak in the turbulent convective region and double peaks in the turbulent diffusion region. The r.m.s. profiles of reactive scalars have simpler forms at the present Damköhler number. However they are not self-similar, especially that of γ_{O_3}, and a similarity solution cannot be found to simplify the problem in modelling.

The gradient model for the turbulent diffusitivity has been checked and it is found that it should work well in the far field of the plume, but in the near field this model will give large errors. It is found that the turbulent diffusitivities obtained from the conserved scalar and reactive scalars are about the same. This is different from Bilger *et al.* (1991) who show that a large difference exists for the turbulent diffusitivities obtained from the conserved scalar and the two reactive scalars. The present data give the non-dimensional turbulent diffusitivity $K/\overline{v'^2}\tau \approx 0.6$, and this is close to the generally used value of 0.5.

Various checks have been made for the capability of the CLA for resolving the length scale of the variance dissipation. Based on these checks the scalar dissipation of the conserved scalar in the near field of the plume has been measured and presented. The data show that the intermittency of the small scales, which are responsible for the scalar dissipation, decreases as the plume develops downstream. The conventional model for the scalar dissipation, i.e. the ratio of the time scale for the energy dissipation to that for the variance dissipation is a constant 2, is not supported in the near field. It is found that this ratio decreases from a value of 5 at $x'/x_0 = 0.05$ to a value of 2 at $x'/x_0 = 0.82$.

Various models used for the closure of the mean chemical reaction rate have been checked. It is found that the product of the means drastically overestimates the mean reaction rate and that a model which interpolates between the frozen and equilibrium limits for the covariance may work better than many of the existing models.

Stochastic mixing models have difficulty in modelling the chemical reaction. One way to model the reactive plume is to combine the stochastic mixing model with the conditional moment closure (CMC) proposed recently by Bilger (1993). The CMC method predicts the conditional mean chemical concentrations very well in the turbulent scalar mixing layer (the conditional mean is defined as the mean of the sub-ensemble which has a given mixture fraction value). Preliminary results from the present reactive plume show that CMC also gives a good prediction of the conditional

mean chemical concentrations. Because the mixture fraction is a conserved scalar and does not depend on chemical reaction, the stochastic mixing model can be used to predict its mean and r.m.s. values. By using an assumed p.d.f. form for the mixture fraction (such as the β-function), the unconditional mean chemical concentrations can be determined by integrating the conditional means weighted by the p.d.f. Further work along this line is in progress.

We would like to thank the Australian Research Council for its financial support of this work.

REFERENCES

ANAND, M. S. & POPE, S. B. 1985 Diffusion behind a line source in grid turbulence. In *Turbulent Shear Flows 4* (ed. L. J. S. Bradbury, F. Durst, B. E. Launder, F. W. Schmidt & T. H. Whitelaw), pp. 46–61. Springer.

BILGER, R. W. 1989 Turbulent diffusion flames. *Ann. Rev. Fluid Mech.* **21**, 101–135.

BILGER, R. W. 1993 Conditional moment closure for turbulent reacting flow. *Phys. Fluids* A **5**, 436–444.

BILGER, R. W., SAETRAN, L. R. & KRISHNAMOORTHY, L. V. 1991 Reaction in a scalar mixing layer. *J. Fluid Mech.* **233** 211–242.

BROWN, R. J. & BILGER, R. W. 1996 An experimental study of a reactive plume in grid turbulence. *J. Fluid Mech.* **312**, 373–407.

CHAMEIDES, W. L. & STEDMAN, D. H. 1977 Tropospheric ozone: coupling transport and photo chemistry. *J. Geophys. Res.* **82**, 1787–1794.

CHATWIN, P. C. & SULLIVAN, P. J. 1990 A simple and unifying physical interpretation of scalar fluctuation measurements from many turbulent shear flows. *J. Fluid Mech.* **212**, 533–556.

CORRSIN, S. 1974 Limitations of gradient transport models in turbulence. *Adv. Geophys.* **18**A, 25–60.

DEARDORFF, J. W. 1978 Closure of second- and third-moment rate equation for diffusion on homogeneous turbulence. *Phys. Fluids* **21**, 525–530.

DEARDORFF, J. W. & WILLS, G. E. 1975 A parameterization of diffusion into the mixing layer. *J. Appl. Met.* **14**, 1451–1458.

DURBIN, P. A. 1980 A stochastic model of two-particle dispersion and concentration fluctuations in homogeneous turbulence. *J. Fluid Mech.* **100**, 279–302.

FACKRELL, J. E. & ROBINS, A. G. 1982 Concentration fluctuations and fluxes in plume from point sources in a turbulent boundary layer. *J. Fluid Mech.* **117**, 1–26.

JAYESH WARHAFT, Z. 1992 Probability distribution, conditional dissipation and transport of passive temperature fluctuations in grid generated turbulence. *Phys. Fluids* A **4**, 2292–2307.

KOMORI, S., HUNT, J. C. R., KANZAKI, T. & MURAKAMI, Y. 1991 The effects of turbulent mixing on the correlation between two species and on concentration fluctuations in non-premixed reacting flows. *J. Fluid Mech.* **228** 629–659.

KOOCHESFAHANI, M. M. & DIMOTAKIS P. E. 1986 Mixing and chemical reactions in a turbulent liquid mixing layer. *J. Fluid Mech.* **170**, 83–112.

LI, J. D. & BILGER, R. W. 1993 Measurement and prediction of the conditional variance in a turbulent reactive scalar-mixing layer. *Phys. Fluids* A **5**, 3255–3264.

LI, J. D. & BILGER, R. W. 1994 A simple theory of conditional mean velocity in turbulent scalar-mixing layer. *Phys. Fluids* A **6**, 605–610.

LI, J. D., BROWN, R. J. & BILGER, R. W. 1992 Experimental study of scalar mixing layer using reactive and passive scalars. In *Proc. Eleventh Australasian Fluid Mechanics Conf., University of Tasmania* (ed. M. R. Davis & G. J. Walker), pp. 159–162.

MOLE, N. & CLARKE, E. D. 1995 Relationships between higher moments of concentration and of dose in turbulent dispersion. *Boundary-Layer Met.* **73**, 35–52.

MOLE, N. & JONES, C. D. 1994 Concentration fluctuation data from dispersion experiments carried out in stable and unstable conditions. *Boundary-Layer Met.* **67**, 41–74.

MONIN, A. S. & YAGLOM, A. M. 1975 *Statistical Fluid Mechanics*, vol. 2. MIT Press.

MUDFORD, N. R. & BILGER, R. W. 1983 A facility for the study of non-equilibrium chemistry in

an isothermal turbulent flow. In *Proc. Eighth Australasian Fluid Mechanics Conf., University of Newcastle.*

MUDFORD, N. R. & BILGER, R. W. 1985 Examination of closure models for mean chemical reaction using experimental data for an isothermal turbulent reacting flow In *20th Symp. (Intl) on Combustion,* pp. 387–394. The Combustion Institute.

POST, K. & KEWLEY, D. J. 1978 Calibration of an ozone calibration reference instrument. *Clean Air* **12**, 2–5.

ROSHKO, A. 1954 On the development of turbulent wakes from vortex streets. *Rep.* 1191. California Institute of Technology.

SAWFORD, B. L. 1992 Spatial structure of concentration moments in homogeneous turbulence. In *10th Symp. on Turbulent and Diffusion. Portland, Oregon,* pp. 180–183. AMS (Boston).

SAWFORD, B. L. & HUNT, J. C. R. 1986 Effects of turbulence structure, molecular diffusion and source size on scalar fluctuation in homogeneous turbulence. *J. Fluid Mech.* **165**, 373–400.

SAWFORD, B. L. & SULLIVAN, P. J. 1995 A simple representation of a developing contaminant concentration field. *J. Fluid Mech.* **289**, 141–157.

STAPOUNTZIS, H. & BRITTER, R. E. 1989 Turbulent diffusion behind a heated line source in a nearly homogeneous turbulent shear flow. In *Turbulent Shear Flow 6* (ed. F. J. Durst, B. E. Launder, F. W. Schmidt & J. H. Whitelaw), pp. 97–108. Springer.

STAPOUNTZIS, H., SAWFORD, B. L., HUNT, J. C. R. & BRITTER, R. E. 1986 Structure of the temperature field downstream of a line source in grid turbulence. *J. Fluid Mech.* **165**, 401–424.

SYKES, R. I., LEWELLEN, W. S. & PARKER, S. F. 1984 A turbulent-transport model for concentration fluctuations and fluxes. *J. Fluid Mech.* **139**, 193–218.

THOMSON, D. J. 1990 A stochastic model for the motion of particle pairs in isotropic high-Reynolds-number turbulence, and its application to the problem of concentration variance. *J. Fluid Mech.* **210**, 113–153.

TOOR, H. C. 1969 Turbulent mixing of two species with and without chemical reaction. *Indust. Engng Chem. Fundam.* **8**, 655–659.

TOOR, H. C. 1993 Effect of chemical reactions on turbulent diffusitivity *AIChE J.* **39**, 1603–1610.

TOWNSEND, A. A. 1954 The diffusion behind a line source in homogeneous turbulence. *Proc. R. Soc. Lond.* A **224**, 487–512.

UBEROI, M. S. & CORRSIN, S. 1952 Diffusion of heat from a line source in isotropic turbulence. *National Advisory Committee for Aeronautics. Tech. Note* 2710.

VEERAVALLI, S. & WARHAFT, Z. 1989 The shearless turbulent mixing layer. *J. Fluid Mech.* **207**, 191–229.

WARHAFT, Z. 1984 The interference of thermal fields from line sources in grid turbulence. *J. Fluid Mech.* **144**, 363–387.

WARHAFT, Z. & LUMLEY, J. L. 1978 An experimental study of the decay of temperature fluctuations in grid turbulence. *J. Fluid Mech.* **88**, 659–684.